

**Tectonic Exhumation of the Central Alps Recorded by Detrital Zircon in the Molasse
Basin, Switzerland**

Owen A. Anfinson^{1,2}, Daniel F. Stockli², Joseph C. Miller³, Andreas Möller³, Fritz Schlunegger⁴

¹Sonoma State University, Department of Geology, Rohnert Park, CA, 94928

²University of Texas at Austin, Department of Geological Sciences, Jackson School of
Geoscience, Austin, TX, 78712

³University of Kansas, Department of Geology, Lawrence, KS

⁴University of Bern, Institute of Geological Sciences, Bern, CH

Correspondence to: Owen A. Anfinson (anfinson@sonoma.edu)

1 **Abstract**

2 Eocene to Miocene sedimentary strata of the Northern Alpine Molasse Basin in
3 Switzerland are well studied, yet they lack robust geochronologic and geochemical analysis of
4 detrital zircon for provenance tracing purposes. Here, we present detrital zircon U-Pb ages
5 coupled with rare earth and trace element geochemistry (petrochronology) to provide insights
6 into the sedimentary provenance and to elucidate the tectonic activity of the central Alpine
7 Orogen from the late Eocene to mid Miocene. Between 35-22.5 ± 1 Ma, the detrital zircon U-Pb
8 age signatures are dominated by age groups of 300-370 Ma, 380-490 Ma, and 500-710 Ma, with
9 minor Proterozoic age contributions. In contrast, from 21.5 ± 1 Ma to ~13.5 Ma (youngest
10 preserved sediments), the detrital zircon U-Pb age signatures were dominated by a 252-300 Ma
11 age group, with a secondary abundance of the 380-490 Ma age group, and only minor
12 contributions of the 500-710 Ma age group. The Eo-Oligocene provenance signatures are
13 consistent with interpretations that initial basin deposition primarily recorded unroofing of the
14 Austroalpine orogenic lid and lesser contributions from underlying Penninic units, containing
15 reworked detritus from Variscan, Caledonian/Sardic, Cadomian, and Pan-African orogenic
16 cycles. In contrast, the dominant 252-300 Ma age group from early Miocene foreland deposits is
17 indicative of the exhumation of Variscan-aged crystalline rocks from upper-Penninic basement
18 units. Noticeable is the lack of Alpine-aged detrital zircon in all samples with the exception of
19 one late Eocene sample, which reflects Alpine volcanism linked to incipient continent-continent
20 collision. In addition, detrital zircon rare earth and trace element data, coupled with zircon
21 morphology and U/Th ratios, point to primarily igneous and rare metamorphic sources.

22 The observed switch from Austroalpine to Penninic detrital provenance in the Molasse
23 Basin at ~22 Ma appears to mark the onset of synorogenic extension of the Central Alps.
24 Synorogenic extension accommodated by the Simplon fault zone promoted updoming and
25 exhumation the Penninic crystalline core of the Alpine Orogen. The lack of Alpine detrital zircon
26 U-Pb ages in all Oligo-Miocene strata corroborate that the Molasse Basin drainage network did
27 not access the prominent Alpine-age Periadriatic intrusions or high-grade metamorphic rocks
28 located in the southern portions of the Lepontine Dome.

29
30
31

32 **1 Introduction**

33 Foreland basins archive the evolution of collisional mountain belts and can provide
34 powerful insights into geodynamic processes operating in the adjacent mountain belt, as the
35 stratigraphy of these basins directly record the history of subduction, thrusting and erosion in the
36 adjacent orogen (Jordan and Flemings, 1991; Sinclair and Allen, 1992; DeCelles and Giles,
37 1996). The Northern Alpine Foreland Basin in Switzerland, also known as the Swiss Molasse
38 Basin, has long been the site of extensive research and helped define fundamental concepts
39 applicable to other flexural foreland basins. Research has focused on sedimentary architecture
40 and facies relationships (Diem, 1986; Platt and Keller, 1992; Kempf et al., 1999; Garefalakis and
41 Schlunegger, 2019), biostratigraphy (Engesser and Mayo, 1987; Schlunegger et al., 1996; Kälin
42 and Kempf, 2009; Jost et al., 2016), and magnetostratigraphy (Schlunegger et al., 1996;
43 Schlunegger et al., 1997a; Kempf et al., 1999; Strunck and Matter, 2002). These studies
44 significantly refined the reconstruction of depositional processes within a detailed temporal
45 framework (Kuhleemann and Kempf, 2002) and yielded a detailed picture of the basin evolution
46 in response to orogenic processes (Sinclair and Allen, 1992; Allen et al., 2013; Schlunegger and
47 Kissling, 2015). However, considerably less attention has been paid to exploring the origins of
48 the sedimentary provenance. Available constraints from heavy mineral assemblages (Fuchtbauer,
49 1964; Gasser, 1966, 1968; Schlanke, 1974; Schlunegger et al., 1997a; Kempf et al., 1999) or
50 clast suites of conglomerates (Habicht, 1945; Matter, 1964; Gasser, 1968; Stürm, 1973;
51 Schlunegger et al., 1997a; Kempf et al., 1999) have largely been inconclusive in terms of
52 sediment sourcing (Von Eynatten et al., 1999). Such insights, however, are of critical importance
53 for reconstructing the causal relationships between orogenic events and the basinal stratigraphic
54 response. In the recent years, advances in isotopic provenance tracing techniques, including
55 detrital mica $^{40}\text{Ar}/^{39}\text{Ar}$ dating (e.g., Von Eynatten et al., 1999; Von Eynatten and Wijbrans,
56 2003), zircon fission-track dating of detrital clasts (Spiegel et al., 2000), detrital garnet and
57 epidote geochemical analysis (Spiegel et al., 2002; Stutenbecker et al., 2019), and detrital zircon
58 U-Pb geochronology (e.g. Malusa et al., 2016; Anfinson et al., 2016; Lu et al., 2018; Sharman et
59 al., 2018a) have offered more quantitative links to Alpine geodynamic processes, revealed
60 through seismic tomography imaging (Lippitsch et al., 2003; Fry et al., 2010; Hetényi et al.,
61 2018) or bedrock geochronology (Boston et al., 2017). In this study, we integrate high-density U-
62 Pb and trace and rare earth element analysis of detrital zircon from the late-Eocene to mid-

63 Miocene stratigraphic record of the Molasse Basin to elucidate the tectonic activity and
64 unroofing history of the Central Alps. We particularly focused in detail on marine and non-
65 marine Molasse deposits of the Lucerne area of central Switzerland (Figure 1) directly north of
66 the Lepontine Dome – the preeminent crystalline core of the central European Alps that exposes
67 Penninic units. These new results document that rapid tectonic unroofing/exhumation of these
68 Penninic rocks in the Lepontine Dome (Boston et al., 2017) resulted in a detectable provenance
69 shift recorded in the foreland basin strata. While signals of this tectonic unroofing/exhumation
70 have been previously documented within the Molasse (e.g., von Eynatten et al., 1999; Spiegel et
71 al., 2000; 2001; 2004; Garefalakis and Schlunegger, 2019), we collected a high sample density
72 detrital zircon U-Pb dataset from marine and non-marine Molasse sandstones near Lucerne
73 (Figure 1) at a temporal resolution of <1 Ma, spanning ~22.5 to 19 Ma. This early Miocene time
74 interval is when a provenance shift was previously documented and we expect to see an abrupt or
75 gradual detrital zircon provenance shift. We augmented the new high-resolution Lucerne dataset
76 with detrital zircon U-Pb ages from western and eastern sections near Thun in Switzerland and
77 Bregenz in Austria (Figure 1), respectively. While these complementary datasets are more
78 limited in terms of temporal resolution, they allow us to explore lateral provenance variations.
79 Overall, this new high-resolution detrital zircon U-Pb dataset from the Northern Alpine Molasse
80 Basin enables us to illuminate erosional processes, syn-tectonic drainage evolution, and linkages
81 to the progressive tectonic unroofing of the orogenic hinterland in the Central Alps as well as to
82 explore the influence of these tectonic processes on the long-term stratigraphic development of
83 the Swiss Molasse Basin.

84

85 **2 The Central Alps: Architecture and Evolution**

86 **2.1 Architecture**

87 The continental collision between Adria, a promontory of the African plate, and the
88 European plate resulted in the Cenozoic Alpine orogen (Stampfli and Borel, 2002; Schmid et al.,
89 2004). Convergence began with the subduction of European oceanic lithosphere beneath the
90 Adriatic continental plate in the Late Cretaceous, resulting in the closure of the Alpine Tethys
91 ocean (Schmid et al., 1996; Lihou and Allen, 1996) and culminating in the final continental
92 collision, which started at ~35 Ma at the latest (Kissling and Schlunegger, 2018). This orogeny
93 resulted in the construction of an ultimately bivergent orogen with the Periadriatic Lineament

94 separating the Northern Alps from the Southern Alps (Schmid et al., 1989). The core of the
95 north- and northwest-vergent Northern Alps is characterized by pervasive Alpine ductile
96 deformation and metamorphism of the basement and associated cover units (Schmid et al.,
97 2004). The south-vergent Southern Alps generally experienced thick- and thin-skinned
98 deformation (Laubscher, 1983) with limited Alpine metamorphic overprinting.

99 The litho-tectonic units of the Northern Alps have been categorized into three broad
100 nappe systems based on their paleogeographic position in Mesozoic times (Figure 1; Schmid et
101 al., 2004; Spiegel et al., 2004). The Helvetic units along the northern margin of the orogen form
102 a stack of thrust sheets that consist of Mesozoic limestones and marls. These sediments
103 accumulated on the stretched (Helvetic units) and distal rifted (Ultrahelvetic units) European
104 continental margin during the Mesozoic phase of rifting and spreading (Schmid et al., 1996;
105 Schmid et al., 2004). The basal thrust of the Helvetic nappes, referred to as the basal Alpine
106 thrust (Figure 1), was folded in response to basement-involved shortening within the European
107 plate at ~20 Ma, resulting in the uplift of the external massifs (Herwegh et al., 2017), exposing
108 Variscan amphibolites and metagranites dated by U-Pb geochronology to 290 to 330 Ma
109 (Schaltegger et al., 2003; von Raumer et al., 2009). The Penninic units represent the oceanic
110 domains of the Piemonte-Liguria and Valais basins, separated by the Briançonnais or Iberian
111 microcontinent (Schmid et al., 1996). The Austroalpine units, both basement and sedimentary
112 cover, formed the northern margin of the Adriatic plate (Pfiffner et al., 2002; Schmid et al.,
113 2004; Handy et al., 2010). While there are few Austroalpine units preserved in the Western and
114 Central Alps, where the exposed rocks belong mainly to the Helvetic and Penninic units, the
115 Austroalpine rocks dominate the Eastern Alps forming an orogenic lid, with Penninic and
116 Helvetic units only exposed in tectonic windows (Figure 1; Schmid et al., 2004). The Lepontine
117 Dome forms the crystalline core of the Penninic nappes and mainly exposes moderate- to high-
118 grade Variscan ortho- and paragneisses separated by Mesozoic metasedimentary slivers (Spicher,
119 1980). Along the western margin, the dome is bordered by the extensional Simplon shear zone
120 and detachment fault (Mancktelow, 1985; Schmid et al., 1996), accommodating tectonic
121 exhumation since ~30 Ma (Gebauer, 1999). Detrital thermochronometric data collected both
122 north and south of the Central Alps have been used to suggest that exhumation rates occurred at
123 a relatively steady state after 15 Ma (Bernet et al., 2001; 2009). However, this notion has been
124 disputed by Carrapa (2010) arguing for exhumation variations directly reflecting the dynamic

125 evolution of the orogenic wedge. Overall rates of synorogenic unroofing of the Lepontine dome
126 appears to have peaked between 20-15 Ma (Grasemann and Mancktelow, 1993; Carrapa, 2009;
127 Boston et al., 2017) on the basis of cooling ages, although rates potentially began to increase prior
128 to 20 Ma as suggested by Schlunegger and Willett (1999), considering a thermal lag time after
129 the onset of faulting.

130

131 **2.2 Pre-Alpine Tectonic Evolution**

132 Since the Neoproterozoic a number of pre-Alpine orogenies contributed to the growth
133 and reworking of the continental crust of the European, Iberian, and Adriatic plates that now
134 make up the Alpine orogen (von Raumer, 1998; Schaltegger and Gebauer, 1999; Schaltegger et
135 al., 2003). As it is important to understand these precursor orogenic events recorded by the
136 detrital zircon data, these orogenic cycles are discussed below from oldest to youngest.

137

138 **2.2.1 Pan-African and Cadomian Orogenies**

139 The Pan-African orogenic cycle refers to a series of protracted late Neoproterozoic
140 orogenic events that resulted in the amalgamation of Gondwana (e.g., Kröner and Stern, 2005).
141 This includes the East African orogen, prominently exposed in the Arabian-Nubian Shield, that
142 resulted in the accretion of predominantly juvenile late Neoproterozoic magmatic crust (750-600
143 Ma) and the ultimate suturing of East and West Gondwana. This juvenile magmatic rocks and
144 older basement of the Saharan Metacraton formed the late Neoproterozoic crust along the
145 northern margin of Gondwana.

146 This margin NE African margin of Gondwana was subsequently overprinted by the
147 Cadomian orogeny. It has been interpreted as an Andean-style Peri-Gondwanan belt that resulted
148 in accretion of island arc and continental margin strata along the Gondwanan continental margin
149 from late Neoproterozoic to Cambrian times (von Raumer et al., 2002; Kröner and Stern, 2004).
150 In general, the age range of this orogenic cycle is overall younger than the Pan-African and
151 broadly spanning 650 to 550 Ma, although some consider the orogenic cycle to encompass a
152 greater timespan of 700-480 Ma (D'Lemos et al., 1990). In the present Alpine orogen, recycled
153 detritus related to the Pan-African and Cadomian orogenies is preserved in the basement units of
154 the Gotthard Massif, Habach complex, and Austro-Alpine Silvretta nappe (Müller et al., 1996),
155 as well as in the Mesozoic and Cenozoic strata of the Schlieren Flysch (Bütler et al., 2011). Pan-

156 African and Cadomian zircon U-Pb crystallization ages, preserved in both the sedimentary and
157 basement units, range from 650 to 600 Ma (Neubauer, 2002). While Cadomian magmatism
158 lasted until at least 520 Ma (Neubauer, 2002), the main phase is roughly synchronous or slightly
159 younger than the Pan-African orogeny (Kröner and Stern, 2004). Hence, early Ediacran detrital
160 zircons are difficult to definitively link to either Pan-African or Cadomian sources, especially as
161 they could be recycled from Paleozoic strata (e.g., Hart et al., 2016; Stephan et al., 2019).

162

163 **2.2.2 Caledonian/Sardic Orogeny**

164 Evidence for Ordovician Caledonian-aged tectonism and magmatism are preserved in all
165 of the major Alpine tectonic units (von Raumer, 1998; Engi et al., 2004). The Aar and Gotthard
166 massifs of central Switzerland (Schaltegger et al., 2003), associated with the European
167 continental lithosphere, as well the Austroalpine Silvretta nappe contain Caledonian-age
168 granitoids (Schaltegger and Gebauer, 1999). In addition, sedimentary units, such as the
169 Ultrahelvtic Flysch, also contain Ordovician detrital zircon grains (Bütler et al., 2011). Although
170 felsic and mafic magmatism and high-pressure metamorphism associated with this Caledonian-
171 aged orogenic cycle (480-450 Ma) are identified in the Alpine basement units, the exact
172 geodynamic setting remains unclear (Schaltegger et al., 2003). While the debate about
173 subduction polarity persists, it is clear crustal fragments were accreted to the Gondwanan margin
174 during the Caledonian orogeny (Schaltegger et al., 2003). While these events have been called
175 Caledonian, they are unlikely associated with the Caledonian (Scandian or Taconic) Orogeny.
176 This has been previously recognized and magmatism has been suggested to be associated with
177 Ordovician-Devonian extensional tectonism along the with Peri-Gondwanan margin of
178 Arabia/NE Africa. Zurbriggen (2017) referred to these events as the Cenerian Orogen, while
179 others studies have referred to it as Sardic (see Stephan et al. 2019b). In many ways, however,
180 this magmatism is a continuation of older Cadomian syn-convergent magmatism along the Peri-
181 Gondwana margin. In order to avoid confusion here, and for simplicity, we will adhere to
182 referring to this as Caledonian-aged rather than Sardic or Cenerian.

183

184 **2.2.3 Variscan Orogeny**

185 While the Pan-African/Cadomian and Caledonian aged orogenies left limited imprints on
186 the Alpine basement, the Variscan orogeny impacted large portions of pre-Alpine crustal

187 basement units in a major way (von Raumer, 1998; von Raumer et al., 2002). The Variscan
188 orogen was the result of the collision between the Gondwana and Laurussia/Avalonia continental
189 plates, which resulted in the formation of the super-continent Pangea (Franke, 2006). The closure
190 of the Paleo-Tethys and the Rheno-Hercynian oceans, leading to the formation of Pangea, started
191 at ~400 Ma and ended in a continent-continent collision at 300 Ma. It was characterized by
192 voluminous syn- and post-orogenic plutonic magmatism (Franke, 2006; von Raumer et al., 2009
193 and references therein). The final stage of post-orogenic Variscan magmatism lasted until ~250
194 Ma (Finger et al., 1997). The Aar and Gotthard external massifs, located south of the central
195 Swiss study location (Figure 1), contain voluminous Variscan U-Pb plutonic rocks (Schaltegger,
196 1994). While the external massifs of the northern part of Central Alps also contain abundant
197 Variscan crustal material (von Raumer et al., 2003; Engi et al., 2004; Franke, 2006), they were
198 not exposed to erosion until ~14 Ma (Stutenbecker et al., 2019).

199

200 **2.2.4 Alpine Orogeny**

201 The collision history between the European and Adriatic continental plates commenced
202 in the Late Cretaceous with the closure of portions of the Alpine Tethys and subduction of the
203 European plate beneath the Adriatic continental plate (Schmid et al., 1996). This Eo-Alpine
204 subduction resulted in blueschist and eclogite facies metamorphism (Ring, 1992; Engi et al.,
205 1995; Rubatto et al., 2011) preserved in slivers between the Penninic nappe stack of the
206 Lepontine (e.g., Cima-Lunga nappe; Schmid et al., 1996). The main Alpine continent-continent
207 collision started at ~33 Ma, when the European continental lithosphere started to enter the
208 subduction channel (Schmid et al., 1996). The buoyancy differences between the oceanic
209 lithosphere and the buoyant continental lithosphere potentially resulted in oceanic slab break-off
210 and at a resulting magmatic flare-up at ~32 Ma (Davis and Blanckenburg, 1995; Schmid et al.,
211 1996). The subsequent advection of heat resulted in a Barrovian-type high-grade metamorphism
212 in the area of the Lepontine dome (Frey et al., 1980; Hurford, 1986; Kissling and Schlunegger,
213 2018).

214 The Helvetic thrust nappes, overthrust by Penninic and Austroalpine nappes prior to the
215 time of slab breakoff, experienced greenschist and prehnite-pumpellyite metamorphism between
216 35 and 30 Ma (Frey et al., 1980; Groshong and Brawn, 1984; Hunziker et al., 1992).

217 Emplacement and thrusting of the Helvetic nappes along the basal Alpine thrust on the proximal
218 European margin (Figure 1) occurred between 25 and 20 Ma and resulted in a greenschist
219 overprint of the basement in the external massifs (Niggli and Niggli, 1965; Frey et al., 1980;
220 Rahn et al., 1994). A late-stage phase of basement-involved duplexing resulted in the rise of the
221 external massifs and the final shape of the Central Alps (Herwegh et al., 2017; Mair et al., 2018;
222 Herwegh et al., 2019).

223

224 **3 Molasse Basin: Architecture, Stratigraphy, and Provenance**

225 The Molasse Basin extends ~600 km from Lake Geneva to the Bohemian massif
226 (Kuhleman and Kempf, 2002; Figure 1). The Swiss part of the Molasse Basin, a sub-section of
227 this foreland trough, is located between Lake Geneva and Lake Constance and is the focus of this
228 study. It is flanked in the north by the Jura Mountains and in the south by the Central Alps. The
229 basin is commonly divided into the Plateau Molasse, the undeformed central basin, and the
230 Subalpine Molasse, the deformed basin adjacent to the Central Alps. The Cenozoic strata of the
231 flexural Swiss Molasse Basin have been divided into five lithostratigraphic units that are (oldest
232 to youngest): the North Helvetic Flysch (NHF), the Lower Marine Molasse (LMM), the Lower
233 Freshwater Molasse (LFM), the Upper Marine Molasse (UMM), and the Upper Freshwater
234 Molasse (UFM) (Figure 2; Sinclair and Allen, 1992). Overall, they record two large-scale
235 shallowing- and coarsening-upward sequences that formed in response to Alpine tectonic
236 processes and changes in sediment supply rates (Matter et al., 1980; Pfiffner, 1986; Sinclair and
237 Allen, 1992; Sinclair et al., 1997; Kuhlemann and Kempf, 2002; Garefalakis and Schlunegger,
238 2018).

239

240 **3.1 North Helvetic Flysch**

241 The earliest foreland basin deposits comprise the North Helvetic Flysch (NHF) with
242 initial turbidite deposition starting in the Middle to Late Eocene (Allen et al., 1991). During that
243 time, clastic deep-water sediments accumulated along the attenuated European continental
244 margin (Crampton and Allen, 1995). The NHF was sourced from the approaching earliest Alpine
245 thrust sheets (Allen et al., 1991). In central Switzerland, the NHF includes sandstone, shale, and
246 some volcanic detritus derived from the volcanic arc situated on the Adriatic plate at that time
247 (Lu et al., 2018; Reichenwallner, 2019). The initial deep-marine, turbiditic clastic deposits

248 exhibit orogen-parallel transport from the west (Sinclair and Allen, 1992). Currently, NHF strata
249 in the region are highly deformed and tectonically located below the Helvetic thrust nappes
250 (Pfiffner, 1986).

251

252 **3.2 Lower Marine Molasse**

253 After deep-marine deposition of the NHF, sedimentation associated with the Lower
254 Marine Molasse (LMM) continued in an underfilled flexural foredeep (Sinclair et al., 1997).
255 From 34-30 Ma (Pfiffner et al., 2002 and references therein) deposition of the LMM
256 progressively transitioned from deep-marine turbidites to tabular and cross-bedded sandstones
257 with symmetrical wave ripples (Matter et al., 1980; Diem, 1986) recording a storm- and wave-
258 dominated shallow-marine environment (Diem, 1986; Schlunegger et al., 2007). The LMM strata
259 record paleocurrent directions that were mostly perpendicular to the orogenic front with a NE-
260 directed tendency (Trümpy et al., 1980; Diem, 1986; Kempf et al., 1999). Sandstone provenance
261 of the LMM suggests mainly derivation from recycled Penninic sedimentary rocks situated along
262 the Alpine front at the time (Matter et al. 1980; Gasser, 1968). Outcrops of the LMM are
263 restricted to the deformed wedge of the Subalpine Molasse.

264 Increased sediment supply in response to rapid erosion of the emerging Alpine orogenic
265 wedge resulted in overfilling of the Swiss Molasse Basin, signaling the shift from the LMM to
266 the fluvial and alluvial deposits of the Lower Freshwater Molasse (LFM) (Sinclair and Allen,
267 1992; Sinclair et al., 1997; Kuhlemann and Kempf, 2002; Schlunegger and Castelltort, 2016;
268 Garefalakis and Schlunegger, 2018). The transition to the LFM was also characterized by the
269 first-appearance of Alpine derived conglomerates at ~30 Ma in central Switzerland (Schlunegger
270 et al., 1997a; Kempf et al., 1999; Kuhlemann and Kempf, 2002).

271

272 **3.3 Lower Freshwater Molasse**

273 Within the Swiss Molasse Basin, the deposition of the Lower Freshwater Molasse (LFM)
274 occurred between ~30 to 20 Ma (Kempf et al., 1999). A regional hiatus separated these older pre-
275 25 Ma (LFM I) from the younger post-24 Ma fluvial deposits (LFM II) (Schlunegger et al.,
276 1997a). In central Switzerland an ~4 km wedge of the LFM is preserved (Stürm, 1973), with the
277 thickest exposed LFM suites occurring in the Subalpine Molasse belt adjacent to the thrust front,
278 such as the Rigi and Höhronen conglomeratic megafans (and others) (Schlunegger et al., 1997b,

279 c). During the ~25-24 Ma hiatus, deposition switched from the Rigi to the Höhronen fan
280 (Schlunegger et al., 1997b, c). Alluvial fan deposition transitioned to channel conglomerates and
281 sandstones away from the thrust front (Büchi and Schlanke, 1977; Platt and Keller, 1992).
282 Limestone, metamorphic, igneous, and ophiolitic clasts derived from the Penninic and
283 Austroalpine units dominated LFM alluvial fan conglomerates (e.g., von Eynatten et al., 1999;
284 Spiegel et al., 2004). Flysch sandstone clasts recycled in the LFM also indicate erosion of older
285 Penninic flysch units (Gasser, 1968). A marked change in clast LFM composition occurred at ~24
286 Ma, with the switch from >80% sedimentary clasts in the Rigi fan prior to 25 Ma (Stürm, 1973)
287 to >50-60% crystalline granitic clasts in the Höhronen fan thereafter (Schlunegger et al., 1997a;
288 Von Eynatten and Wijbrans, 2003). After ~22 Ma, rapid, large-magnitude tectonic exhumation
289 of the Lepontine Dome, in response to syn-orogenic extensions (Mancktelow and Grasemann,
290 1997), led to widespread exposure of the Penninic core complex as evidenced by Alpine-aged
291 detrital mica $^{40}\text{Ar}/^{39}\text{Ar}$ ages in the Molasse Basin (Von Eynatten et al., 1999) and cooling
292 patterns recorded by zircon fission track ages in conglomerate clasts (Spiegel et al., 2000; 2001).
293 At ~21 Ma (LFM IIb), a significant shift in provenance was signaled by a transition in sandstone
294 heavy mineral compositions, as epidote with sources within the Penninic nappes beneath the
295 detachment faults (Spiegel et al., 2002) started to dominate the heavy mineral suite by more than
296 90 percent (Füchtbauer, 1964; Schlanke, 1974; Kempf et al., 1999). This shift was also
297 accompanied by a trend toward more fine-grained sedimentation (Schlunegger et al., 1997a).
298 However, implications of this shift in provenance have been non-conclusive, as Renz (1937),
299 Füchtbauer (1964), and Dietrich (1969) suggested that the epidote minerals were derived from
300 Penninic ophiolites, while Füchtbauer (1964) claimed sourcing from crystalline and greenschist
301 units in the Austroalpine nappes. However, based on Sr and Nd isotopic data from detrital
302 epidote, Spiegel et al., (2002) deduced an ultramafic source for the detrital epidote in all fan
303 systems. They envisioned that in early Miocene times, ophiolitic rocks from the very top of the
304 Penninic nappe stack became unroofed by detachment faults and exposed over large areas of the
305 Central Alps.

306

307 **3.4 Upper Marine Molasse**

308 Continental deposition of the LFM was followed by a shift to marine sedimentation of the
309 Upper Marine Molasse (UMM) in the Swiss foreland basin (Keller, 1989). This has been

310 interpreted as a change back to underfilled conditions. A return towards an underfilled basin
311 started already during LFM times at ~21 and was characterized by a continuous reduction in
312 sediment supply rates (Kuhlemann, 2000; Spiegel et al., 2004; Willett and Schlunegger, 2010).
313 Marine conditions began in the eastern Molasse Basin and propagated westward (Strunck and
314 Matter, 2002; Garefalakis and Schlunegger, 2019). These related effects appear to have been
315 amplified by a tectonically-controlled widening of the basin (Garefalakis and Schlunegger,
316 2019). This change from overfilled non-marine to under-filled marine conditions is referred to as
317 the Burdigalian Transgression (Sinclair et al., 1991). However, the debate continues whether the
318 cause of the Burdigalian Transgression is due to: (i) an increase in sea level outpacing
319 sedimentation (Jin et al., 1995; Zweigel et al., 1998), (ii) an increase in tectonic loading through
320 thrusting of the external massifs (Sinclair et al., 1991), or (iii) an increase in slab pull causing
321 more flexure of the European plate paired with a reduction in sediment supply and a rising
322 eustatic sea level (Garefalakis and Schlunegger, 2019).

323 The Burdigalian Transgression resulted in the deposition of wave and tide-dominated
324 sandstones in a shallow marine environment (Allen et al., 1985; Homewood et al., 1986; Keller,
325 1989; Jost et al., 2016; Garefalakis and Schlunegger, 2019). At the thrust front these shallow-
326 marine sandstones interfinger with fan delta deposits. Shallow-marine deposition lasted until ~17
327 Ma (Schlunegger et al., 1997c). Heavy mineral data (Allen et al., 1985) and clast petrography
328 analysis (Matter, 1964), in conjunction with measurements of clast orientations in conglomerates
329 and cross-beds in sandstones (Allen et al., 1985; Garefalakis and Schlunegger, 2019), reveal that
330 the UMM of Switzerland was a semi-closed basin. Detritus sourced from the Central Alps was
331 deposited adjacent to the fan deltas and reworked by waves and tidal currents.

332

333 **3.5 Upper Freshwater Molasse**

334 The Upper Freshwater Molasse (UFM) consists of non-marine conglomerates and
335 sandstones deposited in prograding alluvial fans and fluvial floodplains (Keller, 2000). The
336 thickest section of the preserved UFM (~1500 m) is situated to the west of Lucerne (Matter,
337 1964; Trümpy, 1980). Geochemistry of detrital garnet in the UFM record the first signal of
338 erosion of the external massifs by ~14 Ma at the latest (Stutenbecker et al., 2019).

339 Deposition of the UFM in central Switzerland is only recorded until ~12 Ma
340 (Schlunegger et al., 1996) as younger strata were eroded from the region (e.g. Burkhard and

341 Sommaruga, 1998; Cederbom et al., 2004; Cederbom et al., 2011). Vitritine reflectance and
342 apatite fission track borehole data from the Molasse Basin suggest that up to 700 m of UFM
343 strata were removed by erosion (Schegg et al., 1999; Cederbom et al., 2004; 2011). Erosion of
344 the basin fill started in the Late Miocene to Pliocene (Mazurek et al., 2006; Cederbom et al.,
345 2011) after active thrusting propagated to the Jura Mountains, and the Molasse Basin essentially
346 became a piggy-back basin (Burkhard and Sommaruga, 1998; Pfiffner et al., 2002), or
347 alternatively a negative alpha basin (Willett and Schlunegger, 2011).

348

349 **4 Sampling Strategy and Methodology**

350 **4.1 Sampling Strategy**

351 Samples were collected along the southern portion of the basin within the Plateau
352 Molasse, the Subalpine Molasse, and the North Helvetic Flysch. Three sections were sampled:
353 The Lucerne Section in central Switzerland, the Thun Section in west-central Switzerland, and
354 the Bregenz Section in westernmost Austria (Figures 1 and 3; Table 1). Sampling in the Lucerne
355 Section was accomplished to cover the full range in depositional ages from the North Helvetic
356 Flysch to the Upper Freshwater Molasse, spanning between 34 and 13.5 Ma with less than a 2-5
357 myr time resolution. For the ~22.5 to 19 Ma time interval within the Lucerne Section, our high-
358 density strategy sampled at a temporal resolution of <1 Ma. Sample sites in the Bregenz Section
359 covered the major lithostratigraphic groups of the Molasse deposits at a lower resolution, while
360 samples from the Thun Section comprised only the LFM and terrestrial equivalents of the UMM
361 deposits for along-strike comparison purposes. All separated samples contained detrital zircon
362 and were used for U-Pb age dating. Stratigraphic age assignments for the samples for the
363 Lucerne Section were based on the chronological framework from Schlunegger et al. (1997a),
364 established in the Lucerne area through detailed magneto- and biostratigraphy (e.g., Weggis,
365 Rigi, and Höhrone conglomerates; LFM I and LFM IIa/IIb units). Ages were projected into the
366 Lucerne Section through mapping and balanced cross section restorations. Chronostratigraphic
367 age constraints for the UMM sandstones were taken from Keller (1989), Jost et al. (2016) and
368 Garefalakis and Schlunegger (2019). Precise ages for the UFM units are not available and they
369 could comprise the entire range between 17 Ma (base of UFM) and ~13 Ma (youngest LFM
370 deposits in Switzerland; Kempf and Matter (1999)). The chronological framework for the
371 Molasse units for the Thun section is based on litho- and chronostratigraphic work by

372 Schlunegger et al. (1993, 1996). There, OA13- samples were collected along the
373 magnetostratigraphic section of Schlunegger et al. (1996) with an age precision of ~0.5 Ma.
374 Sample site 10SMB07 was collected from a conglomerate unit, mapped (Beck and Rutsch, 1949)
375 as a terrestrial equivalent of the UMM (Burdigalian), although the depositional age could also
376 correspond to the UFM (Langhian), as indicated by litho- and seismostratigraphic and heavy
377 mineral data from a deep well (Schlunegger et al., 1993). Site 10SMB06 comprises a suite of
378 conglomerates with quartzite clasts - their first appearance was dated to ~25 Ma in the adjacent
379 thrust sheet to the South (Schlunegger et al., 1996). While, deposition of quartzite clasts,
380 however, continues well into the UFM (Matter, 1964), the quartzite conglomerates in the Thun
381 section (10SMB06) directly overly sandstones of the LMF II as a tectonic interpretation of a
382 seismic section has revealed (Schlunegger et al., 1993). Therefore, we tentatively assigned an
383 LMF II age to the 10SMB06 sample site. Finally, sampling and stratigraphic age assignments for
384 samples from the Bregenz Section were guided by the geological map of Oberhauser (1994) and
385 by additional chronologic (Kempf et al., 1999) and stratigraphic work (Schaad et al., 1992). We
386 considered an uncertainty of ± 2 Ma to the age assignment for the Bregenz Section samples.

387

388 **4.2 Zircon U-Pb LA-ICPMS Methodology**

389 The bulk of the detrital zircon samples were analyzed at the UTChron geochronology
390 facility in the Department of Geological Sciences at the University of Texas at Austin and a
391 smaller subset at the at the Isotope Geochemistry Lab (IGL) in the Department of Geology at the
392 University of Kansas, using identical instrumentation and very similar analytical procedures, but
393 different data reduction software (Table 1). All samples underwent conventional heavy mineral
394 separation, including crushing, grinding, water-tabling, magnetic, and heavy liquid separations,
395 but no sieving at any point. Separate zircon grains were mounted on double-sided tape (tape-
396 mount) on a 1” acrylic or epoxy disc without polishing. For all samples 120-140 grains were
397 randomly selected for LA-ICPMS analysis to avoid biases and capturing all major age
398 components (>5%) (Vermeesch, 2004). All grains were depth-profiled using a Photon Machines
399 Analyte G2 ATLex 300si ArF 193 nm Excimer Laser combined with a ThermoElement 2 single
400 collector, magnetic sector -ICP-MS, following analytical protocols of Marsh and Stockli (2015).
401 30 seconds of background was measured followed by 10 pre-ablation “cleaning” shots, then 15
402 sec of washout to measure background, prior to 30 sec of sample analysis. Each grain was

403 ablated for 30 seconds using a 30 μm spot with a fluence of $\sim 4 \text{ J/cm}^2$, resulting in $\sim 20 \text{ }\mu\text{m}$ deep
404 ablation pits. For U-Pb geochronologic analyses of detrital zircon the masses ^{202}Hg , ^{204}Pb , ^{206}Pb ,
405 ^{207}Pb , ^{208}Pb , ^{232}Th , ^{235}U , and ^{238}U were measured.

406 GJ1 was used as primary zircon standard ($^{206}\text{Pb}/^{238}\text{U}$ $601.7 \pm 1.3 \text{ Ma}$, $^{207}\text{Pb}/^{206}\text{Pb}$ 607 ± 4
407 Ma; Jackson et al. 2004) and interspersed every 3-4 unknown analyses for elemental and depth-
408 dependent fractionation. Plesovice ($337.1 \pm 0.4 \text{ Ma}$, Slama et al., 2008) was used as a secondary
409 standard for quality control, yielding $^{206}\text{Pb}/^{238}\text{U}$ ages during this study of $338 \pm 6 \text{ Ma}$, which is in
410 agreement with the published age. No common Pb correction was applied. At UTChron, data
411 reduction was performed using the IgorPro (Paton et al., 2010) based Iolite 3.4 software with
412 Visual Age data reduction scheme (Petrus & Kamber, 2012), while at KU's IGL U-Pb data were
413 reduced using Papiage (Dunkl et al., 2009) or Iolite employing an Andersen (2002) correction
414 method and decay constants from (Steiger and Jäger, 1977). The Andersen (2002) correction
415 method iteratively calculates the $^{208}\text{Pb}/^{232}\text{Th}$, $^{207}\text{Pb}/^{235}\text{U}$, and $^{206}\text{Pb}/^{238}\text{U}$ ages to correct for
416 common-Pb where ^{204}Pb cannot be accurately measured. Sample 09SFB11 was reduced using
417 Papiage and for this reason U ppm and U/Th ratio were not calculated.

418 All uncertainties are quoted at 2σ and age uncertainty of reference materials are not
419 propagated. For ages younger than 850 Ma, $^{206}\text{Pb}/^{238}\text{U}$ ages are reported and grains were
420 eliminated from text and figures if there was greater than 10% discordance between the
421 $^{206}\text{Pb}/^{238}\text{U}$ age and the $^{207}\text{Pb}/^{235}\text{U}$ age or the $^{206}\text{Pb}/^{238}\text{U}$ age had greater than 10% 2σ absolute
422 error. For ages older than 850 Ma, $^{207}\text{Pb}/^{206}\text{Pb}$ ages are reported and grains were eliminated from
423 text and figures if there was greater than 20% discordance between $^{206}\text{Pb}/^{238}\text{U}$ age and
424 $^{207}\text{Pb}/^{206}\text{Pb}$ age. Analytical data were visually inspected for common Pb, inheritance, or Pb loss
425 using the VisualAge live concordia function (Petrus and Kamber, 2012). Laser Ablation-ICPMS
426 depth profiling allows for the definition of more than one age from a single grain, hence ages in
427 Supplemental File 1 are labelled either single age, rim, or core. Commonly a single concordant
428 age was obtained for each zircon; however, if more than one concordant age was defined then
429 both analyses were included in the data reporting.

430

431 **4.3 Laser Ablation-Split Stream (LASS) Analyses of Detrital Zircon**

432 In an attempt to glean additional provenance constraints from Molasse samples, we also
433 combined U-Pb with trace element (TE) and rare earth element (REE) analyses on the same

434 grain for select samples via laser ablation split-steam (LASS) U-Pb analysis at the University of
435 Texas at Austin (Marsh and Stockli, 2015). Combined U-Pb isotopic and TE/REE data can help
436 improve provenance resolution on the basis of petrogenic affiliations of individual grains
437 (Kylander-Clark et al., 2013). For LASS analysis, ablated aerosols were divided between two
438 identical ThermoFisher Element2 single collector, magnetic sector-ICP-MS instruments and
439 analyzed for ^{29}Si , ^{49}Ti , ^{89}Y , ^{137}Ba , ^{139}La , ^{140}Ce , ^{141}Pr , ^{146}Nd , ^{147}Sm , ^{153}Eu , ^{157}Gd , ^{159}Tb , ^{163}Dy ,
440 ^{165}Ho , ^{166}Er , ^{169}Tm , ^{172}Yb , ^{175}Lu , ^{178}Hf , ^{181}Ta , ^{232}Th , and ^{238}U . Data generated from the TE and
441 REE analyses were reduced using the “Trace_Elements_IS” data reduction scheme from Iolite
442 (Paton et al., 2011), using ^{29}Si as an internal standard indexed at 15.3216 wt.% ^{29}Si . NIST612
443 was used as the primary reference material and GJ1 and Pak1 as secondary standards to verify
444 data accuracy.

445

446 **4.4 Zircon Elemental Analysis**

447 While studies (e.g. Hoskin and Ireland, 2000; Belousova et al., 2002) have shown that
448 zircon REE patterns in general do not show systematic diagnostic variations as a function of
449 different continental crustal rock types (von Eynatten and Dunkl, 2012), it has been shown that
450 TE and REE can be used to differentiate between igneous zircon from continental (e.g., arc),
451 oceanic, and island arc tectono-magmatic environments (Grimes et al., 2015). Furthermore, trace
452 elements and REEs can be used to fingerprint zircon with mantle affinity (i.e., kimberlites and
453 carbonatites; Hoskin and Ireland, 2000), hydrothermal zircon (Hoskin, 2005), or zircon that grew
454 or recrystallized under high-grade metamorphic conditions (Rubatto, 2002). Furthermore, Ce and
455 Eu anomalies in zircons have been used as proxies for magmatic oxidation states (Trail et al.,
456 2012; Zhong et al., 2019) and Ti-in-zircon as a crystallization thermometer (Watson et al., 2006).
457 Detrital studies have utilized these techniques to identify characteristic zircon signatures from
458 non-typical sources (e.g. Anfinson et al., 2016; Barber et al., 2019).

459 Chondrite-normalized REE zircon signatures were only considered for concordant U-Pb
460 ages as metamictization likely also affected REE and TE spectra. Zircon with anomalously
461 elevated and flat LREE (La-Gd) concentrations were excluded from figures and interpretations
462 as these are likely due to mineral inclusions (i.e. apatite) or hydrothermal alteration (Bell et al.,
463 2019).

464

465 **5 Detrital U-Pb Age Groups and Associated Orogenic Cycles**

466 In an attempt to simplify data presentation and data reporting, the detrital zircon U-Pb
467 ages were lumped into genetically-related tectono-magmatic age groups that include the
468 Variscan, Caledonian/Sardic, and Cadomian/Pan-African orogenic cycles. In addition to these
469 three pre-Alpine orogenic cycles we also considered the total number of Cenozoic (Alpine) ages,
470 Mesozoic (Tethyan) ages, and pre-Cadomian ages. The following sections provide a brief
471 description of the different delineated age groups. While there can be considerable debate
472 regarding the exact duration of orogenic cycles (Dewey and Horsfield, 1970), grouping zircon U-
473 Pb ages according to their tectono-magmatic or orogenic affinity provides a convenient way to
474 discuss potential detrital sources. The informal age ranges adopted in this study are Cenozoic (0
475 to 66 Ma), Mesozoic (66 to 252 Ma), late Variscan (252 to 300 Ma), early Variscan (300-370
476 Ma) Caledonian age (370 to 490 Ma), Cadomian/Pan-African (490 to 710 Ma), and Pre-
477 Cadomian (>710 Ma). We simplified these age groups to represent a continuous series with no
478 time gaps and to ensure no omission of ages and for simplicity of depicting ages using the
479 DetritalPy software of Sharman et al. (2018b). Abundant Variscan zircon U-Pb ages are split into
480 two groups (late Variscan and early Variscan) to reflect differences between syn- and post-
481 orogenic magmatism on the basis of discussion of Finger et al. (1997). Finger et al. (1997) noted
482 five generalized genetic groups of granitoid production during the Variscan Orogeny: 1) Late-
483 Devonian to Early Carboniferous I-type granitoids (370 to 340 Ma), 2) Early Carboniferous
484 deformed S-type granitoids (~340 Ma), 3) Late Visian-Early Namurian S-type and high-K I-type
485 granitoids (340 Ma to 310 Ma), 4) Post-collisional I-type granitoids and tonalites (310-290 Ma),
486 and 5) Late Carboniferous to Permian leucogranites (300-250 Ma). The general age ranges of
487 the Caledonian/Sardic (370 to 490 Ma) and Cadomian/Pan African (490 to 710 Ma) orogens are
488 based on Pfiffner (2014), McCann (2008), Krawczyk et al. (2008), and Stephan et al. (2019).
489 While uncertainties and discordance of LA-ICPMS U-Pb ages allow for overlap between these
490 groupings, they provide a potential and viable way to depict and estimate detrital zircon
491 contributions from these different source regions and to identify potential provenance changes in
492 the Molasse Basin.

493

494 **6 Detrital Zircon U-Pb Ages**

495 **6.1 Lucerne Section (Central Switzerland; Sample Locations: Figure 3a; U-Pb Data: Figure**
496 **4)**

497 For data presentation, we grouped the detrital zircon U-Pb ages according to their
498 lithostratigraphic units for simplicity as there is little variation in DZ U-Pb age signatures within
499 individual units. The detrital zircon U-Pb ages of individual samples can be found in
500 Supplemental File 1 and all associated sample information can be found in Table 1.

501

502 **6.1.1 Northern Helvetic Flysch (NHF)**

503 Samples 09SFB43 and 09SFB02 were collected from the Northern Helvetic Flysch and
504 have a depositional age of 35 ± 3 Ma. The samples contain a total of 261 concordant U-Pb ages
505 ranging from 34.8 to 2838 Ma and can be binned in the following tectono-magmatic groups
506 discussed in the Section 4: Cenozoic (4.2%), Mesozoic (0.8%), Late Variscan (9.6%), Early
507 Variscan (5%), Caledonian (29.1%), Cadomian (37.9%), and pre-Cadomian (13.4%). Notably,
508 there are eleven grains with ages between 34.8 and 37.3 Ma in sample 09SFB43 that fall within
509 uncertainty of the depositional age.

510

511 **6.1.2 Lower Marine Molasse**

512 Sample 09SFB10b was collected from the Lower Marine Molasse and has a depositional
513 age of 32 ± 1 Ma. The sample contains a total of 114 concordant U-Pb zircon ages ranging from
514 243.6 to 2611 Ma. There were no Cenozoic grains, two Mesozoic ages at 243.6 and 243.7 Ma
515 and two Permian ages at 287.2 and 294.6. The age spectrum is composed of the following age
516 groups with the following percentages: Mesozoic (1.8%), Late Variscan (1.8%), Early Variscan
517 (17.5%), Caledonian (36%), Cadomian (23.7%), and pre-Cadomian (19.3%).

518

519 **6.1.3 Lower Freshwater Molasse**

520 Samples 09SFB45 and 09SFB21 were collected from the lower units of the Lower
521 Freshwater Molasse and have depositional ages of 27 ± 1 Ma (LFM I) and 22.5 ± 1 Ma (LFM
522 IIa), respectively. The combined samples contain a total of 202 concordant ages ranging from
523 191.7 to 2821 Ma. The sample yielded no Cenozoic grains and four Mesozoic grains with ages
524 ranging from 191.7 to 243.1 Ma. The rest of the grains fall into the following age groups

525 Mesozoic (2%), Late Variscan (9.4%), Early Variscan (13.9%), Caledonian (25.7%), Cadomian
526 (26.2%), and Pre-Cadomian (19.3%).

527 Samples 09SFB13, 09SFB08 and 09SFB33 were collected from Unit IIB of the Lower
528 Freshwater Molasse and have depositional ages of 21.5 ± 1 Ma, 21.5 ± 1 Ma and 21 ± 1 Ma,
529 respectively. The combined samples contain a total of 505 concordant U-Pb analyses ranging in
530 age from 222.7 to 2700 Ma. There were not Cenozoic ages and eleven Triassic ages ranging
531 from 222.7 Ma to 251.6 Ma - 9 of these 11 grains had >900 ppm U and were considered suspect
532 for possible Pb loss. The age spectrum is composed of the following age groups and proportions:
533 Mesozoic (2%), Late Variscan (53.3%), Early Variscan (10.5%), Caledonian (15.0%), Cadomian
534 (11.7%), and Pre-Cadomian (7.3%).

535

536 **6.1.5 Upper Marine Molasse**

537 Samples 09SFB05, 09SFB29, 09SFB49, and 09SFB14 were collected from the Upper
538 Marine Molasse and have depositional ages of 20 ± 1 Ma, 19 ± 1 Ma, 19 ± 1 Ma, and 17.5 ± 1
539 Ma, respectively. These combined samples contain a total of 356 concordant ages ranging in age
540 from 162.1 Ma to 2470 Ma. There are no Cenozoic grains, two Jurassic ages (162.1 Ma and
541 165.9 Ma) and seventeen Triassic ages that range from 210.7 Ma to 251.6 Ma. Overall, these
542 ages fall into the following groups: Mesozoic (5.3%), Late Variscan (41.1%), Early Variscan
543 (14.3%), Caledonian (13.8%), Cadomian (15.7%), and Pre-Cadomian (6.7%).

544

545 **6.1.6 Upper Freshwater Molasse**

546 Samples 09SFB12, 09SFB07, 09SFB11, and 09SFB38 were all collected from the Upper
547 Freshwater Molasse and have depositional ages of 16 ± 1 Ma, 15.5 ± 1 Ma, 14 ± 1 Ma, and 13.5
548 ± 1 Ma, respectively. These combined samples contain a total of 364 concordant ages ranging
549 from 30.6 Ma to 3059.9 Ma and yielded a single Cenozoic age (30.6 Ma), a single Cretaceous
550 age (130.7 Ma), a single Jurassic age (148.3 Ma), and fourteen Triassic ages that range from
551 207.8.7 Ma to 251.7 Ma. Overall, the age groups are characterized by the following proportions:
552 Cenozoic (0.3%), Mesozoic (4.4%), Late Variscan (36%), Early Variscan (20%), Caledonian
553 (18.4%), Cadomian (14%), and Pre-Cadomian (6.9%).

554

555 **6.2 Thun Section (West-Central Switzerland; Sample Locations: Figure 3b; U-Pb Data:**
556 **Figure 5)**

557 **6.2.1 Lower Freshwater Molasse**

558 Samples 13SFB03, 13SFB04, and 10SMB06 were collected from the Lower Freshwater
559 Molasse and have depositional ages of 28 ± 0.5 Ma, 26 ± 0.5 Ma and 22 ± 2.5 Ma, respectively.
560 The combined samples contain a total of 344 concordant ages ranging from 217.8 to 3304 Ma,
561 falling into the following age groups: Mesozoic (2%), Late Variscan (18%), Early Variscan
562 (23%), Caledonian (26.2%), Cadomian (20.9%), and Pre-Cadomian (9.9%).

563

564 **6.2.2 Terrestrial Equivalents of the Upper Marine Molasse and Upper Freshwater Molasse**

565 Sample 10SMB07 was collected from the terrestrial equivalent of the Upper Marine
566 Molasse and Upper Freshwater Molasse and has a depositional age of 18 ± 3 Ma. A large
567 number of grains were discordant and hence the sample yielded only a total of 53 concordant
568 ages ranging from 186.1 to 2688.2 Ma. The age groups represented were Mesozoic (3.8%), Late
569 Variscan (49.1%), Early Variscan (22.6%), Caledonian (9.4%), Cadomian (7.5%), and Pre-
570 Cadomian (7.5%).

571

572 **6.3 Bregenz Section (Western Austria; Sample Locations: Figure 3c; U-Pb Data: Figure 6)**

573 **6.3.1 Lower Marine Molasse**

574 Sample 10SMB12 was collected from the Lower Marine Molasse and has a depositional
575 age of 32 ± 2 Ma. The sample contains a total of 98 concordant ages ranging from 36.3 to 2702
576 Ma. It was characterized by the age groups and percentages: Cenozoic (1%), Mesozoic (1%),
577 Late Variscan (7.1%), Early Variscan (13.3%), Caledonian (17.3%), Cadomian (25.5%), and
578 Pre-Cadomian (34.7%). Remarkable was an anomalously large percentage of Mesoproterozoic
579 (11.2%) and Paleoproterozoic (12.2%) ages.

580

581 **6.3.2 Lower Freshwater Molasse**

582 Sample 10SMB11 was collected from the Lower Freshwater Molasse and has a
583 depositional age of 22 ± 2 Ma. The sample contains a total of 70 concordant ages ranging from
584 217.5 to 2172 Ma, falling into the following groups with the following percentages: Mesozoic

585 (1.4%), Late Variscan (12.9%), Early Variscan (27.1%), Caledonian (27.1%), Cadomian
586 (14.3%), and Pre-Cadomian (17.1%).

587

588 **5.3.3 Upper Marine Molasse**

589 Sample 10SMB10 was collected from the Upper Marine Molasse and has a depositional
590 age of 19 ± 2 Ma. The sample contains a total of 161 concordant ages ranging from 234.3 to
591 2837 Ma. It is characterized by the following age group and percentages: Mesozoic (0.8%), Late
592 Variscan (13.7%), Early Variscan (21.1%), Caledonian (24.2%), Cadomian (19.9%), and Pre-
593 Cadomian (20.5%).

594

595 **6.3.3 Upper Freshwater Molasse**

596 Sample 10SMB09 was collected from the Upper Freshwater Molasse and has a
597 depositional age of 15 ± 2 Ma. The sample contains a total of 81 concordant ages ranging from
598 257.7.3 to 2030 Ma, characterized by the following age groups and percentages: Late Variscan
599 (12.3%), Early Variscan (48.1%), Caledonian (11.1%), Cadomian (16%), and Pre-Cadomian
600 (12.3%). Notably, the sample lacked any Cenozoic or Mesozoic zircons.

601

602 **7 Detrital Zircon Geochemistry and Rim-Core relationships**

603 Individual zircon grains often record multiple growth episodes in response to magmatic
604 or metamorphic events within a single source terrane. Recovery of these multi-event source
605 signatures from a single zircon allow for improved pinpointing of detrital provenance and a more
606 completing understanding of the source terrane history. Laser-Ablation Split-Stream (LASS)
607 Depth Profiling by ICP-MS has enabled for a more systematic harvesting of these relationships
608 and hence complete picture of the growth of the detrital zircon grains (e.g. Anfinson et al. 2016;
609 Barber et al. 2019). We applied this to methodology to samples of the Lucerne Section following
610 the analytical procedures of Marsh and Stockli (2015) and Soto-Kerans et al. (2020). For
611 discussion purposes, these data were divided into two groups: (1) depositional ages >22 Ma and
612 (2) depositional ages <22 Ma. For depositional ages >22 Ma, the geochemical data were drawn
613 from the REE analyses of four samples (approximate depositional age in parentheses): 09SFB33
614 (21 Ma), 09SFB49 (19 Ma), 09SFB14 (17.5 Ma), and 09SFB38 (13.5 Ma). For depositional ages
615 >22 Ma, the geochemical data were drawn from samples 09SFB45 (27 Ma) and 09SFB21 (22.5

616 Ma). Detrital zircon grains that have experienced hydrothermal alteration or contamination of the
617 zircon profile by exotic mineral inclusion (e.g. apatite) commonly show high, flat light rare earth
618 element (LREE) patterns (Hoskin and Ireland, 2000; Bell et al., 2019). We have removed these
619 altered profiles from the data plots but show all data in Supplemental File 2.

620

621 **7.1 Depositional Ages >22 Ma**

622 The REE data show that Variscan detrital zircons are mainly magmatic in origin as
623 indicated by comparison to REE profiles from Belousova et al. (2002) and Hoskin and Ireland
624 (2000). There is little to no evidence for metamorphic/metasomatic zircon grains (Figure 7a). In
625 contrast, Cadomian and in particular Caledonian zircon grains exhibit elevated U-Th values
626 (Figure 8b). Only a single Caledonian grain with a 468 Ma U-Pb age (sample SFB21) is
627 characterized by a depleted HREE profile (Fig 7c) indicative of metamorphic growth in the
628 presence of garnet (e.g. Rubatto, 2002). There is little evidence of mafic zircon sources, as the U
629 ppm and TE values and typically more characteristic of arc magmatism (e.g. Grimes et al. 2015;
630 Barber et al., 2019). For depositional ages older than 22 Ma there is a minor number of Variscan
631 rims on Cadomian and Caledonian cores (Figure 9).

632

633 **7.2 Depositional Ages <22 Ma**

634 Similar to the pre-Miocene detrital zircon, LASS-ICP-MS geochemical data from the
635 younger stratigraphic samples (<22 Ma) suggest that Variscan detrital zircons are primarily of
636 magmatic origin. However, compared to the older samples, there is evidence for increasing input
637 of metamorphic/metasomatic grains (Figure 7b). Sample 09SFB14 contained one Variscan grain
638 (262 Ma U-Pb age) and the youngest Molasse sample (09SFB38; ca. 13.5 Ma) three Variscan
639 zircons (316-329 Ma) with depleted HREE profiles. 09SFB38 also has a higher percentage of
640 Variscan grains with elevated U/Th values (Figure 8a). Together, these data indicate a slight
641 increase in the input of metamorphic Variscan sources through time. However, there is no
642 evidence for the input of neither magmatic nor metamorphic Alpine zircons or zircon rims.

643 The geochemical data of Caledonian and Cadomian detrital zircons from these Miocene
644 samples also are consistent with primarily a magmatic origin with a subordinate number of
645 detrital zircon grains exhibiting elevated U/Th values (Figure 8b). However, there is little
646 evidence for metamorphic grains from the REE profiles (Figure 7d).

647 Overall, the vast majority of all detrital zircon grains are interpreted to have a typical
648 magmatic REE profile, with positive Ce and negative Eu anomalies, and overall positive slopes,
649 including positive MREE-HREE slopes. The U/Th from all detrital zircon grains are consistent
650 with predominately magmatic characters. In summary, the REE data suggest that detrital zircons
651 from all recent orogenic cycles are primarily magmatic in origin with very limited metamorphic
652 zircon input. For depositional ages younger than 22 Ma there is a noticeable increase in Variscan
653 rims on Caledonian, Cadomian, and older Proterozoic cores (Figure 9).

654

655 **8 Discussion**

656 Erosion scenarios for the Alps that emphasize the importance of tectonic exhumation of
657 the Lepontine Dome have previously been proposed on the basis of provenance signals in the
658 Molasse Basin, such as detrital zircon fission track data or detrital zircon and epidote
659 geochemistry. These data and lines of evidence were synthesized by Spiegel et al. (2004). These
660 reconstructions, however, have been based on a combination of various provenance indicators
661 and at a relatively low temporal resolution in the Molasse Basin. This study leverages a detailed
662 zircon U-Pb and trace element dataset that focuses on foreland basin strata due north of the
663 Lepontine Dome with samples collected at high (<1 Myrs) temporal stratigraphic resolution.
664 Hence, the progressive changes observed in the detrital zircon U-Pb age patterns in the Molasse
665 Basin of central Switzerland allow for direct and high-resolution insights into the reconstruction
666 of the evolution of drainage networks of the Central Alps and the driving forces during the
667 Alpine orogenesis, particularly in the Early Miocene between ~ 23 and 18 Ma when a
668 provenance shift and arrival of a Lepontine source signal (Boston et al., 2017) for the Molasse
669 Basin has been observed (Spiegel et al., 2004). Central to this discussion is the salient observation
670 that within the Lucerne Section a remarkable shift is observed in the detrital zircon U-Pb age
671 signatures at ~ 22 Ma. Prior to that time, detrital zircon ages included the entire range of pre-
672 Cadomian, Cadomian, Caledonian, Variscan ages in similar proportions (Figure 4). In addition,
673 there was little variation in zircon age patterns from sample to sample in the Molasse strata
674 deposited prior to 22 Ma. Noteworthy is the occurrence of ~34 Ma detrital zircon in the North
675 Helvetic Flysch sample 09SFB43, these ages are essentially contemporaneous with the
676 depositional age and make up ~8% of the detrital zircon grains (Figure 4). If Alpine age detrital
677 zircon was present in other Molasse Basin samples it would have been identified due to the depth

678 profile analytical approach (where rims can easily be recognized during data reduction). The lack
679 of these Alpine ages in the Molasse sediments, and the lack of these ages in modern River
680 sediments (e.g. Krippner et al. 2013) suggests that the drainage divide has likely remained north
681 of Tertiary intrusives exposed along the Periadriatic Lineament.

682 In contrast to underlying strata, after 22 Ma, detrital zircon ages are dominated by late
683 Variscan ages and limited contributions of older detrital zircon grains. The trend of increasing
684 late Variscan ages is nicely depicted in the Multidimensional Scaling Plot (MDS) of Figure 10.
685 Figure 10 compares the statistical similarity of the samples to one another utilizing an MDS plot
686 with pie diagrams (Generated using the DetritalPy software of Sharman et al. (2018b) and based
687 of methods described in Vermeesch (2018)). This change in age pattern is rather abrupt and was
688 likely accomplished within one million years. The zircon REE chemistry data (Figures 7 and 8)
689 suggest that the bulk of the detrital zircon grains in the Cenozoic Molasse strata were primarily
690 derived from magmatic or meta-magmatic rocks. However, after ~22 Ma there appears to have
691 been a slight increase in the input of Variscan and Caledonian metamorphic sources. In the next
692 section, we present a scenario of how this abrupt change can possibly be linked to the tectonic
693 exhumation of the region surrounding the Lepontine Dome, the most likely sediment source for
694 the central Swiss Molasse (Schlunegger et al., 1998; Von Eynatten et al., 1999). This provenance
695 scenario, presented in chronological order, also includes consideration of the apparent first-cycle
696 zircon grains (~34 Ma) encountered in the Eocene North Helvetic Flysch. The provenance of the
697 detrital zircon grains is thus discussed within a geodynamic framework of the Alpine orogeny.

698

699 **8.1 Eocene Drainage Divide During Deposition of the North Helvetic Flysch**

700 The subduction of the European plate beneath the Adriatic plate began in the Late
701 Cretaceous and was associated with the closure of the Tethys and Valais oceans (Schmid et al.,
702 1996). The subducted material mainly included Tethyan oceanic crust, parts of the Valais oceans,
703 and continental crustal slivers of the Briannçonnais or Iberian microcontinent (Schmid et al.,
704 1996; Kissling and Schlunegger, 2018). The introduction of the European plate into the
705 subduction channel resulted in high-pressure metamorphic overprints of these rocks. Subduction
706 of the oceanic crust resulted in the down-warping of the European plate and the formation of the
707 Flysch trough, where clastic turbidites sourced from the erosion of the Adriatic orogenic lid were
708 deposited in a deep-marine trench on the distal European plate (Sinclair et al., 1997). This also

709 includes the volcano-clastic material of the Taveyannaz sandstone (Sinclair et al., 1997; Lu et al.,
710 2018) and the related 34 Ma first-cycle volcanic zircon grains encountered in the Eocene North
711 Helvetic Flysch. Hence, while arc magmatism was situation on the Adriatic continental upper
712 plate, volcanoclastic material was shed into the flysch trough on the European continental
713 margin. This implies that during Flysch sedimentation, the N-S drainage divide was likely
714 situated somewhere within the Adriatic upper plate margin.

715

716 **8.2 Abrupt Oligo-Miocene Detrital Zircon U-Pb Provenance Shift**

717 Between 35 and 32 Ma, buoyant material of the European continental crust entered the
718 subduction channel (Schmid et al., 1996; Handy et al., 2010). Strong tensional forces between
719 the dense and subducted oceanic European lithosphere and the buoyant European continental
720 crust possibly resulted in the break-off of the oceanic plate. As a result, the European plate
721 experienced a phase of rebound and uplift, which was accomplished by back-thrusting along the
722 Periadriatic Lineament (Schmid et al., 1989) and progressive ductile thrusting and duplexing of
723 the deeper Penninic domain (e.g., Wiederkehr et al. 2009; Steck et al., 2013). Although this
724 model has recently been challenged based on zircon U-Pb and Hf isotopic compositions from the
725 Tertiary Periadriatic intrusives (Ji et al., 2018), it still offers the most suitable explanation of the
726 Alpine processes during the Oligocene (Kissling and Schlunegger, 2018). In response, the
727 topographic and drainage divide shifted farther north to the locus of back-thrusting. Streams
728 reestablished their network and eroded the Alpine topography through headward retreat, thereby
729 rapidly eroding and downcutting into deeper crustal levels from the Austroalpine cover nappes
730 and into the Penninic units (Figure 11a; Schlunegger and Norton, 2013). This is indicated by an
731 increase of crystalline clasts in the conglomerates of the Lower Freshwater Molasse (Gasser,
732 1968; Stürm, 1973) and it is reflected by the detrital zircon U-Pb ages characterized by a
733 cosmopolitan spectra that span the entire spread from Cadomian and older to late Variscan zircon
734 grains (Figure 10).

735 Surface uplift and progressive erosional unroofing also resulted in a steadily increasing
736 sediment flux into the Molasse Basin (Kuhlemann, 2000; Willett and Schlunegger, 2010) and a
737 continuous increase in plutonic and volcanic clasts in the conglomerates (Stürm, 1973; Kempf et
738 al., 1999) throughout the Oligocene (Figure 11b). However, this pattern fundamentally changed
739 at ~22-20 Ma when rapid slip along the Simplon fault occurred (Schlunegger and Willett, 1999),

740 resulting in the rapid exhumation of the Lepontine dome as recorded by currently exposed rocks
741 (Figure 11c; Boston et al., 2017). Although thermal modeling and heavy mineral
742 thermochronometric data imply that fastest cooling occurred between ~ 20-15 Ma (Campani et
743 al., 2010; Boston et al., 2017), tectonic exhumation likely started prior to this time interval given
744 the lag time of isotherm perturbations at upper crustal levels (Schlunegger and Willet, 1999). In
745 contrast to Schlunegger et al. (1998), Von Eynatten et al. (1999) and Spiegel et al., (2000; 2001)
746 suggested, on the basis of detrital mica $^{40}\text{Ar}/^{39}\text{Ar}$ age patterns and zircon cooling ages of detrital
747 material, that slip along the Simplon normal fault did not result in a major change of the Alpine
748 drainage organization, and that the Lepontine was still a major sediment source for the Molasse
749 Basin even after the period of rapid updoming and exhumation. In the Lucerne Section,
750 contemporaneous changes included: (i) a shift in the petrographic composition of conglomerates
751 with igneous constituents starting to dominate the clast suite (Schlunegger et al., 1998), (ii) a
752 shift toward predominance of epidote in the heavy mineral spectra (Gasser, 1966) with sources
753 from nappes beneath the detachment faults (Spiegel et al., 2002), (iii) a continuous decrease in
754 sediment discharge (Kuhlemann, 2000) paired with a fining-upward trend in the 22-20 Ma
755 fluvial sediments of the LFM (Schlunegger et al., 1997a), and (iv) a return from terrestrial (LFM)
756 back to marine (UMM) sedimentation at ~20 Ma within an underfilled flexural foreland basin
757 (Keller, 1989; Garefalakis and Schlunegger, 2019). Our new detrital zircon U-Pb ages exhibit by
758 an abrupt shift towards detrital zircon signatures dominated by Variscan zircons (Figure 10),
759 supporting the earlier notion of erosion of deeper crustal levels in response to tectonic
760 exhumation (Spiegel et al., 2004). Because the Lucerne Section was situated due north of the
761 Lepontine dome, and since this area was a major source of sediment for the Molasse Basin even
762 after this phase of rapid tectonic exhumation (Von Eynatten et al., 1999; Spiegel et al., 2004), we
763 consider that these detrital zircon grains were most likely sourced from this part of the Central
764 Alps. The shift to predominantly Variscan age zircon grains in UFM deposits is also observed in
765 the western Swiss Molasse Basin (Thun Section; Figure 5 and 10), which hosts conglomerate
766 and sandstone that were derived both from the footwall and the hanging wall of the Simplon
767 detachment fault (Matter, 1964; Schlunegger et al., 1993; Eynatten et al., 1999). A similar related
768 signal was also identified in the axial drainage of the Molasse ~200 km farther east in the
769 submarine Basal Hall Formation (~20 Ma) (Sharman et al., 2018a).

770

771 **8.3 Constrains on surface exhumation of external massifs**

772 It has been suggested that rapid rock uplift of the external Aar Massif (Figure 1), which is
773 in close proximity to the Thun and Lucerne sections, likely started at ~20 Ma (Herwegh et al.,
774 2017; 2019). However, we do not see a related signal in the detrital zircon U-Pb age patterns
775 (Figure 10). Based on geochemical data of detrital garnet, Stutenbecker et al. (2019) showed that
776 the first crystalline material of the Alpine external massifs became exposed to the surface no
777 earlier than ~14 Ma, with the consequence that related shifts were not detected in the zircon age
778 populations. In fact, low-temperature thermochronometric data from the Aar and Mont Blanc
779 Massifs (e.g. Vernon et al., 2009; Glotzbach et al., 2011) document a major exhumation phase of
780 the external massifs in the latest Miocene and early Pliocene, likely related to out-of-sequence
781 thrusting and duplexing at depth. It is therefore likely, that surface exposure of the external
782 massifs might not have occurred until the late Miocene-early Pliocene.

783

784 **8.4 Continuous detrital-zircon age evolution in eastern Molasse Basin**

785 The detrital zircon ages of the sediments collected in the eastern region of the Swiss
786 Molasse (Bregenz Section; Figure 1 and 3c) show a shift where the relative abundance of
787 Variscan material continuously increased through time (Figures 6 and 10). The material of this
788 region was derived from the eastern Swiss Alps, which includes the Austroalpine units, and
789 possibly the eastern portion of the Lepontine Dome (Kuhlemann and Kempf, 2002). This area
790 was not particularly affected by tectonic exhumation (Schmid et al., 1996). Therefore, we
791 interpret the continuous change in the age populations as record of a rather normal unroofing
792 sequence into the Alpine edifice.

793

794 **8.5 Tectonic exhumation and relationships to decreasing sediment flux**

795 The overall decrease in sediment discharge, which contributed to the transgression of the
796 Upper Marine Molasse (Garefalakis and Schlunegger, 2019), could be related to the tectonic
797 exhumation of the Lepontine Dome. In particular, slip along the Simplon detachment fault
798 resulted in the displacement of a ca. 10 km-thick stack of rock units within a few million years
799 (Schlunegger and Willett, 1999; Campani et al., 2010). A mechanism such as this is expected to
800 leave a measurable impact on a landscape, which possibly includes (i) a reduction of the overall
801 topography in the region of the footwall rocks (provided not all removal of rock was

802 compensated by uplift), (ii) a modification and thus a perturbation of the landscape
803 morphometry, particularly in the footwall of a detachment fault (Pazzaglia et al., 2007), and (iii)
804 exposure of rock with a higher metamorphic grade and thus a lower bedrock erodibility (Kühni
805 and Pfiffner, 2001). We lack quantitative data to properly identify the main driving force and
806 therefore consider that the combination of these three effects possibly contributed to an overall
807 lower erosional efficiency of the Alpine streams, with the consequence that sediment flux to the
808 Molasse decreased for a few million years. We thus use these mechanisms, together with the
809 larger subsidence (Garefalakis and Schlunegger, 2019), to explain the shallowing-upward fluvial
810 deposition in the post 22 Ma LFM and the transgression of the UMM. Low sediment supply
811 prevailed until steady state erosional conditions were re-established during deposition of the
812 UFM, as implied by the increase in sediment discharge to pre-20 Ma conditions towards the end
813 of the UMM (Kuhleemann, 2000).

814

815 **9 Conclusions**

816 During deposition of the LFM, at ~22 Ma, detrital zircon U-Pb ages record decreased
817 contributions from Austroalpine cover nappes and erosion into crystalline basement of the
818 Penninic nappes. Erosional mechanisms mainly occurred as normal unroofing process through
819 continuous dissection into the Alpine edifice. The abrupt shift in the age populations of detrital
820 zircon at ~22 Ma reflected in the Central Swiss Molasse indicates a phase of fast tectonic
821 exhumation of the Lepontine Dome. Molasse sediments that were derived from the lateral
822 margin of the Lepontine area (Thun and Bregenz Sections) were less affected by this phase of
823 rapid tectonic exhumation, and age populations record a more continuous unroofing sequence.
824 Tectonic exhumation was associated with a drop in sediment supply to the Molasse, fining
825 upward trends and contributed to the establishment of shallow marine conditions. This could
826 reflect the shift towards a less erosive landscape where tectonic exhumation resulted in a
827 reduction of relief and exposure of rocks with low erodibility.

828

829 **Data Availability:** Due to the nature of the U-Pb and Geochemistry data (LASS and Depth
830 Profiled), the data have been included in a supplemental document and are not uploaded to
831 Geochron.org

832

833 **Supplemental Files:**

834 Supplemental File 1: All depth profiled detrital zircon U-Pb data. (includes Rim-Core distinction
835 that is not allowed on Geochron.org

836 Supplemental File 2: All Geochemistry data from LASS analysis. This Geochem data also
837 includes the associated ages from Supplemental File 1.

838

839 **Author Contributions:**

840 **OA:** As primary author OA collected samples, analyzed samples at UTChron, led the writing of
841 the manuscript, and assembled collaborators.

842 **DS:** DS collected a number of the samples, analyzed some samples with JM and AM at the
843 University of Kansas, helped analyze samples at UTChron, and aided in the writing of the
844 manuscript

845 **JM:** JM collected a number of the samples with DS, wrote his Master's Thesis at KU on the U-
846 Pb and (U-Th)/He at KU, and aided in the writing of the manuscript.

847 **AM:** AM was advisor to JM at KU during his masters work, he analyzed a number of the U-Pb
848 samples at KU, and aided in the writing of the manuscript.

849 **FS:** FS helped with sample collection, met for a field trip in Switzerland, provided expertise on
850 the Molasse and Alpine Orogen, and aided in the writing of the manuscript.

851 **Competing Interests:** The authors declare that they have no conflict of interest

852

853 **Acknowledgements**

854 Thanks to the Jackson School of Geoscience at the University of Texas at Austin and to
855 Sonoma State University for financial support. We would like to thank Lisa Stockli and Des
856 Patterson for help with laboratory work at UTChron. Thanks to Andrew Smye, Jeff Marsh, Ryan
857 Mackenzie, and Shannon Loomis and for extensive discussion of the research project.

858

859 **Table and Figure Captions**

860 **Tables**

861 **Table 1.** Sample Information. Depositional age errors are based on: Lucerne Section-
862 Schlunegger et al. (1997a); Thun Section- Schlunegger et al. (1993; 1996); Bregenz Section-
863 Oberhauser (1994), Kempf et al. (1999), and Schaad et al. (1992). 'X' in 'U-Pb' and 'Geochem'

864 columns indicate data available for that sample. Final column indicates if samples were analyzed
865 at either the University of Kansas (KU) or the University of Texas at Austin (UT). Errors for
866 depositional ages are discussed in Section 3. Corresponding methods are found in the Section 4.

867

868 **Figures**

869 **Figure 1.** Geologic map of the Central Alps and Swiss Molasse Basin highlighting geologic
870 features and paleogeographic units discussed in the text (map is adapted from Garefalakis and
871 Schlunegger (2019) and based on: Froitzheim et al. (1996), Schmid et al. (2004), Handy et al.
872 (2010), and Kissling and Schlunegger (2018). Locations are shown for the Lucerne Section,
873 Thun Section, and Bregenz Section that are highlighted in Figures 3a, 3b, and 3c, respectively.

874

875 **Figure 2.** Generalized stratigraphy of the Molasse Basin. Modified from Miller (2009) and
876 (Keller, 2000).

877

878 **Figure 3.** Stratigraphic units and sample locations of the three sampled sections A) Lucerne
879 Section: geologic map and cross section modified from (Schlunegger et al., 1997a). In both the
880 map and the simplified cross section, sample numbers are only the last two digits of the sample
881 numbers from Table 1. B) Thun Section: geologic map modified from Schlunegger et al. (1993;
882 1996). C) Bregenz Section: geologic map simplified from Oberhauser, (1994), Kempf et al.,
883 (1999), and Schaad et al. (1992).

884

885 **Figure 4.** Detrital zircon U-Pb age data from the Lucerne Section (locations of samples depicted
886 in Figure 3a) plotted as Kernel Density Estimations (KDE; Bandwidth set to 10), a Cumulative
887 Distribution Plot (CDP), and as pie diagrams. Colored bars in the KDE and colored wedges in
888 the pie diagrams show the relative abundance of age groups discussed in Section 5. Samples
889 associated with each unit are referenced in Table 1. Plot only shows ages from 0-1000 Ma;
890 however, a small number of older ages were analyzed and that data can be found in
891 Supplemental File 1. N= (Number of samples, number of ages depicted/ total number of total
892 ages).

893

894 **Figure 5.** Detrital zircon U-Pb age data from the Thun Section (locations of samples depicted in
895 Figure 3b). See Figure 4 legend and caption for additional information.

896

897 **Figure 6.** Detrital zircon U-Pb age data from the Bregenz Section (locations of samples depicted
898 in Figure 3c). See Figure 4 legend and caption for additional information.

899

900 **Figure 7.** Detrital zircon rare earth element (REE) spider diagram for samples collected from the
901 Lucerne Section. (A) Variscan U-Pb ages and REE data for samples younger than a 22 Ma
902 depositional age and (B) older than a 22 Ma depositional age. (C) Caledonian and Cadomian U-
903 Pb ages and REE data for samples younger than a 22 Ma depositional age and (D) older than a
904 22 Ma depositional age. For plots A and C the geochemical data is drawn from samples SFB33
905 (21 Ma), SFB49 (19Ma), SFB14 (17.5 Ma), and SFB38 (13.5 Ma). For B and D the geochemical
906 data is drawn from samples SFB21 (22.5 Ma) and SFB45 (27 Ma). The data suggest that detrital
907 zircons from all three recent orogenic cycles record primarily grains that are magmatic in origin
908 (Belousova et al., 2002; Hoskin and Ireland, 2000), with little evidence of
909 metamorphic/metasomatic grains. Data can be found in Supplemental File 2.

910

911 **Figure 8.** Age vs U/Th comparison for detrital zircon grains with depositional ages older than 22
912 Ma and younger than 22 Ma. A) Variscan aged grains, B) Caledonian and Cadomian age grains.
913 Although not definitive, grains with elevated U/Th (or low Th/U; e.g. Rubatto et al. 2002) have a
914 higher likelihood of being metamorphic in origin. There are few Variscan grains with elevated
915 U/Th from both the pre- and post-22 Ma depositional ages, suggesting little input of
916 metamorphic sources for these ages. There are a large number of Caledonian and a handful of
917 Cadomian grains with elevated U/Th from both the pre- and post-22 Ma depositional ages,
918 indicating metamorphic sources for these age grains are prevalent.

919

920 **Figure 9.** Rim vs core ages for detrital zircon grains from samples with depositional ages older
921 than 22 Ma and younger than 22 Ma from the Lucerne Section. Prior to the 22 Ma transition in
922 source area there is a minor number of Variscan rims on Cadomian and Caledonian cores. In

923 samples younger than 22 Ma there is a noticeable increase in Variscan rims on Caledonian,
924 Cadomian, and Proterozoic cores. Error bars are 2 sigma non-propagated errors.

925

926 **Figure 10.** Multidimensional Scaling Plot (MDS) of detrital zircon U-Pb ages for all units from
927 the Molasse Basin. The MDS plot was produced with the DetritalPy software of Sharman et al.
928 (2018b) and is based on methods outlined by Vermeesch (2018). Pie diagram colors correspond
929 to age groups from Figure 4 and ages discussed in Section 4.

930

931 **Figure 11.** Schematic cross-section through the central Alps of Switzerland, illustrating the
932 development of the Alpine relief and the topography through time. A) 30 Ma-25 Ma: Slab
933 breakoff resulted in backthrusting along the Periadriatic fault and in the growth of the Alpine
934 topography. The erosional hinterland was mainly made up of the Austroalpine cover nappes
935 (Adriatic plate) and Penninic sedimentary rocks at the orogen front. B) 25 Ma: Ongoing surface
936 erosion resulted in the formation of an Alpine-type landscape with valleys and mountains. First
937 dissection into the crystalline core of the European continental plate was registered by the first
938 arrival of Penninic crystalline material in the foreland basin sometime between 25 and 22 Ma,
939 depending on the location within the basin. 22 Ma was also the time when sediment discharge to
940 the Molasse was highest. Tectonic exhumation through slip along the Simplon fault started to
941 occur at the highest rates. C) 20 Ma: Tectonic exhumation along the Simplon fault resulted in
942 widespread exposure of high-grade rocks, in a shift in the clast suites of the conglomerates and in
943 a change in the detrital zircon age signatures. Faulting along the detachment fault most likely
944 subdued the topography in the hinterland. As a result, sediment flux to the Molasse Basin
945 decreased, and the basin became underfilled and was occupied by the peripheral sea of the Upper
946 Marine Molasse. (Figures based on restored sections by Schlunegger and Kissling, 2015).

947

948 **References**

949 Allen P.A., Mange-Rajetzky M., Matter A., Homewood P.: Dynamic palaeogeography of
950 the open Burdigalian seaway, Swiss Molasse basin. *Eclogae Geol. Helv.*, 78, 351–381, 1985.

951 Allen, M., Saville, C., Blanc, E. P., Talebian, M., and Nissen, E.: Orogenic plateau
952 growth: Expansion of the Turkish-Iranian Plateau across the Zagros fold-and-thrust belt,
953 *Tectonics*, 32, 171-190, 2013.

954 Allen, P. A., Crampton, S. L., and Sinclair, H. D.: The inception and early evolution of
955 the North Alpine Foreland Basin, Switzerland, *Basin Research*, 3, 143-163, 1991.

956 Andersen, T.: Correction of common lead in U–Pb analyses that do not report ^{204}Pb ,
957 *Chemical geology*, 192, 59-79, 2002.

958 Anfinson, O. A., Malusà, M. G., Ottria, G., Dafov, L. N., and Stockli, D. F.: Tracking
959 coarse-grained gravity flows by LASS-ICP-MS depth-profiling of detrital zircon (Aveto
960 Formation, Adriatic foredeep, Italy), *Mar Petrol Geol*, 77, 1163-1176, 2016.

961 Barber, D. E., Stockli, D. F., and Galster, F.: The Proto-Zagros Foreland Basin in
962 Lorestan, Western Iran: Insights From Multiminerale Detrital Geothermochronometric and Trace
963 Elemental Provenance Analysis, *Geochemistry, Geophysics, Geosystems*, 20, 2657-2680, 2019.

964 Beck, P. und Rutsch, R. F.: *Geol. Atlasblatt 21 (1:25,000) Münsingen—Konolfingen—*
965 *Gerzensee—Heimberg, Schweiz. Geol. Komm*, 1949.

966 Bell, E. A., Boehnke, P., Barboni, M., and Harrison, T. M.: Tracking chemical alteration
967 in magmatic zircon using rare earth element abundances, *Chemical Geology*, 510, 56-71, 2019.

968 Belousova, E., Griffin, W. L., O'Reilly, S. Y., and Fisher, N.: Igneous zircon: trace
969 element composition as an indicator of source rock type, *Contributions to mineralogy and*
970 *petrology*, 143, 602-622, 2002.

971 Bernet, M., Zattin, M., Garver, J. I., Brandon, M. T., and Vance, J. A.: Steady-state
972 exhumation of the European Alps, *Geology*, 29, 35-38, 2001.

973 Bernet, M., Brandon, M., Garver, J., Balestieri, M., Ventura, B., and Zattin, M.:
974 Exhuming the Alps through time: Clues from detrital zircon fission-track thermochronology,
975 *Basin Research*, 21, 781-798, 2009.

976 Boston, K. R., Rubatto, D., Hermann, J., Engi, M., and Amelin, Y.: Geochronology of
977 accessory allanite and monazite in the Barrovian metamorphic sequence of the Central Alps,
978 Switzerland, *Lithos*, 286, 502-518, 2017.

979 Büchi, U. P., and Schlanke, S.: Zur paläogeographie der schweizerischen Molasse, *Erdöl-*
980 *Erdgas-Zeitschrift*, 93, 57-69, 1977.

981 Burkhard, M., and Sommaruga, A.: Evolution of the western Swiss Molasse basin:
982 structural relations with the Alps and the Jura belt, Geological Society, London, *Special*
983 *Publications*, 134, 279-298, 1998.

984 Bütler, E., Winkler, W., and Guillong, M.: Laser ablation U/Pb age patterns of detrital
985 zircons in the Schlieren Flysch (Central Switzerland): new evidence on the detrital sources,
986 Swiss Journal of Geosciences, 104, 225, 2011.

987 Campani, M., Herman, F., and Mancktelow, N.: Two- and three-dimensional thermal
988 modeling of a low-angle detachment: Exhumation history of the Simplon Fault Zone, central
989 Alps, Journal of Geophysical Research: Solid Earth, 115, 2010.

990 Carrapa, B.: Tracing exhumation and orogenic wedge dynamics in the European Alps
991 with detrital thermochronology, Geology, 37, 1127-1130, 2009.

992 Carrapa, B.: Tracing exhumation and orogenic wedge dynamics in the European Alps
993 with detrital thermochronology: REPLY, Geology, 38, e227-e227, 2010.

994

995 Cederbom, C. E., Sinclair, H. D., Schlunegger, F., and Rahn, M. K.: Climate-induced
996 rebound and exhumation of the European Alps, Geology, 32, 709-712, 2004.

997 Cederbom, C. E., Van Der Beek, P., Schlunegger, F., Sinclair, H. D., and Oncken, O.:
998 Rapid extensive erosion of the North Alpine foreland basin at 5–4 Ma, Basin Research, 23, 528-
999 550, 2011.

1000 Crampton, S., and Allen, P.: Recognition of forebulge unconformities associated with
1001 early stage foreland basin development: example from the North Alpine Foreland Basin, AAPG
1002 bulletin, 79, 1495-1514, 1995.

1003 D'Lemos, R., Strachan, R., and Topley, C.: The Cadomian orogeny in the North
1004 Armorican Massif: a brief review, Geological Society, London, Special Publications, 51, 3-12,
1005 1990.

1006 Davis, J. H., and Blanckenburg, F.: Slab breakoff: A model of lithosphere detachment
1007 and its test in the magmatism and deformation of collisional orogens, Earth and Planetary
1008 Science Letters, 129, 85-102, 1995.

1009 DeCelles, P. G., and Giles, K. A.: Foreland basin systems, Basin research, 8, 105-123,
1010 1996.

1011 Dewey, J., and Horsfield, B.: Plate tectonics, orogeny and continental growth, Nature,
1012 225, 521-525, 1970.

1013 Diem, B.: Die Untere Meeresmolasse zwischen der Saane (Westschweiz) und der Ammer
1014 (Oberbayern), Eclogae Geol Helv, 79, 493-559, 1986.

1015 Dietrich, V.: Die Oberhalbsteiner Talbildung im Tertiär: ein Vergleich zwischen den
1016 Ophiolithen und deren Detritus in der ostschweizerischen Molasse, Geologisches Institut der
1017 Eidg. Technischen Hochschule und der Universität, 1969.

1018 Dunkl, I., Mikes, T., Frei, D., Gerdes, A., von Eynatten, H.: PepiAGE data reduction
1019 program for time-resolved U/Pb analyses – introduction and call for tests and discussion.
1020 University of Goettingen Publication, p. 15, 2009.

1021 Engesser, B., and Mayo, N. A.: A biozonation of the Lower Freshwater Molasse
1022 (Oligocene and Aagenian) of Switzerland and Savoy on the basis of fossil mammals., Münchner
1023 Geowiss, 10, 67-84, 1987.

1024 Engi, M., Todd, C., and Schmatz, D.: Tertiary metamorphic conditions in the eastern
1025 Lepontine Alps, Schweizerische Mineralogische und Petrographische Mitteilungen, 75, 347-369,
1026 1995.

1027 Engi, M., Bousquet, R., and Berger, A.: Explanatory notes to the map: Metamorphic
1028 structure of the Alps-Central Alps, Mitteilungen der Österreichischen Mineralogischen
1029 Gesellschaft, 149, 157-173, 2004.

1030 Finger, F., Roberts, M., Haunschmid, B., Schermaier, A., and Steyrer, H.-P.: Variscan
1031 granitoids of central Europe: their typology, potential sources and tectonothermal relations,
1032 Mineralogy and Petrology, 61, 67-96, 1997.

1033 Franke, W.: The Variscan orogen in Central Europe: construction and collapse,
1034 Geological Society, London, Memoirs, 32, 333-343, 2006.

1035 Frey, M., Teichmiüller, M., Teichmiüller, R., Mullis, J., Kfinzi, B., Breitschmid, A.,
1036 Gruner, U., and Schwitzer, B.; Very low grade metamorphism in external parts of the Central
1037 Alps: Illite crystallinity, coal rank and fluid inclusion data, Eclogae Geol. Helv., 73, 173-203,
1038 1980.

1039 Froitzheim, N., Schmid, S. M., and Frey, M.: Mesozoic paleogeography and the timing of
1040 eclogite-facies metamorphism in the Alps: a working hypothesis, Eclogae Geol Helv, 89, 81-&,
1041 1996.

1042 Fry, B., Deschamps, F., Kissling, E., Stehly, L., and Giardini, D.: Layered azimuthal
1043 anisotropy of Rayleigh wave phase velocities in the European Alpine lithosphere inferred from
1044 ambient noise, Earth and Planetary Science Letters, 297, 95-102, 2010.

1045 Fuchtbauer, H.: Sedimentpetrographische Untersuchungen in der alteren Molasse
1046 nordlich der Alpen, *Eclogae Geol. Helv.*, 57, 157-298, 1964.

1047 Garefalakis, P., and Schlunegger, F.: Stratigraphic architecture of the Upper Marine
1048 Molasse implies incipient westward tilt of the foreland plate, *Poster GeoBonn*, 2018.

1049 Gasser, U.: Sedimentologische Untersuchungen in der äusseren Zone der subalpinen
1050 Molasse des Entlebuch (Kt. Luzern), Verlag nicht ermittelbar, 1966.

1051 Gasser, U.: Die innere Zone der subalpinen Molasse des Entlebuch (Kt. Luzern):
1052 Geologie und Sedimentologie, Birkhäuser, 1968.

1053 Gebauer, D.: Alpine geochronology of the Central and Western Alps: new constraints for
1054 a complex geodynamic evolution, *Schweizerische Mineralogische und Petrographische*
1055 *Mitteilungen*, 79, 191-208, 1999.

1056 Glotzbach, C., Van Der Beek, P. A., and Spiegel, C.: Episodic exhumation and relief
1057 growth in the Mont Blanc massif, Western Alps from numerical modelling of thermochronology
1058 data, *Earth and Planetary Science Letters*, 304, 417-430, 2011.

1059 Grasemann, B., and Mancktelow, N. S.: Two-dimensional thermal modelling of normal
1060 faulting: the Simplon Fault Zone, Central Alps, Switzerland, *Tectonophysics*, 225, 155-165,
1061 1993.

1062 Grimes, C., Wooden, J., Cheadle, M., and John, B.: “Fingerprinting” tectono-magmatic
1063 provenance using trace elements in igneous zircon, *Contributions to Mineralogy and Petrology*,
1064 170, 46, 2015.

1065 Habicht, K.: Neuere Beobachtungen in der subalpinen Molasse zwischen Zugersee und
1066 dem st. gallischen Rheintal, *Geologisches Institut der Eidg. Technischen Hochschule und der*
1067 *Universität*, 1945.

1068 Handy, M. R., Schmid, S. M., Bousquet, R., Kissling, E., and Bernoulli, D.: Reconciling
1069 plate-tectonic reconstructions of Alpine Tethys with the geological–geophysical record of
1070 spreading and subduction in the Alps, *Earth-Science Reviews*, 102, 121-158, 2010.

1071 Hart, N. R., Stockli, D. F., and Hayman, N. W.: Provenance evolution during progressive
1072 rifting and hyperextension using bedrock and detrital zircon U-Pb geochronology, *Mauléon*
1073 *Basin, western Pyrenees*, *Geosphere*, 12, 1166-1186, 2016.

1074 Herwegh, M., Berger, A., Baumberger, R., Wehrens, P., and Kissling, E.: Large-scale
1075 crustal-block-extrusion during late Alpine collision, *Scientific reports*, 7, 1-10, 2017.

1076 Herwegh, M., Berger, A., Glotzbach, C., Wangenheim, C., Mock, S., Wehrens, P.,
1077 Baumberger, R., Egli, D., and Kissling, E.: Late stages of continent-continent collision: Timing,
1078 kinematic evolution, and exhumation of the Northern rim (Aar Massif) of the Alps, *Earth-science*
1079 *reviews*, 102959, 2019.

1080 Hetényi, G., Molinari, I., Clinton, J., Bokelmann, G., Bondár, I., Crawford, W. C., Dessa,
1081 J.-X., Doubre, C., Friederich, W., and Fuchs, F.: The AlpArray seismic network: a large-scale
1082 European experiment to image the Alpine Orogen, *Surveys in geophysics*, 39, 1009-1033, 2018.

1083 Homewood, P., Allen, P., and Williams, G.: Dynamics of the Molasse Basin of western
1084 Switzerland, in: *Foreland basins*, Spec. Publ. Int. Ass. Sediment, 199-217, 1986.

1085 Hoskin, P. W., and Ireland, T. R.: Rare earth element chemistry of zircon and its use as a
1086 provenance indicator, *Geology*, 28, 627-630, 2000.

1087 Hoskin, P. W.: Trace-element composition of hydrothermal zircon and the alteration of
1088 Hadean zircon from the Jack Hills, Australia, *Geochimica et Cosmochimica Acta*, 69, 637-648,
1089 2005.

1090 Hunziker, J. C., Desmons, J., and Hurford, A. J.: Thirty-two years of geochronological
1091 work in the Central and Western Alps: a review on seven maps, 1992.

1092 Hurford, A. J.: Cooling and uplift patterns in the Lepontine Alps South Central
1093 Switzerland and an age of vertical movement on the Insubric fault line *Contributions to*
1094 *Mineralogy and Petrology*, 92, 413-427, 1986.

1095 Jin, J., Aigner, T., Luterbacher, H., Bachmann, G. H., and Müller, M.: Sequence
1096 stratigraphy and depositional history in the south-eastern German Molasse Basin, *Mar Petrol*
1097 *Geol*, 12, 929-940, 1995.

1098 Jordan, T., and Flemings, P. B.: Large-scale stratigraphic architecture, eustatic variation,
1099 and unsteady tectonism: a theoretical evaluation, *Journal of Geophysical Research: Solid Earth*,
1100 96, 6681-6699, 1991.

1101 Jost, J., Kempf, O., and Kälin, D.: Stratigraphy and palaeoecology of the Upper Marine
1102 Molasse (OMM) of the central Swiss Plateau, *Swiss Journal of Geosciences*, 109, 149-169, 2016.

1103 Kälin, D., and Kempf, O.: High-resolution stratigraphy from the continental record of the
1104 Middle Miocene Northern Alpine Foreland Basin of Switzerland, *Neues Jahrbuch für Geologie*
1105 *und Paläontologie-Abhandlungen*, 254, 177-235, 2009.

1106 Keller, B.: Fazies und Stratigraphie der Oberen Meeresmolasse (Unteres Miozän)
1107 zwischen Napf und Bodensee. Unpubl. PhD Thesis, Universität Bern, Bern, 402 p, 1989.

1108 Keller, B.: Fazies der Molasse anhand eines Querschnitts durch das zentrale Schweizer
1109 Mittelland, Jber. Mitt. Oberrhein, 82, 55-92, 2000.

1110 Kempf, O., Matter, A., Burbank, D., and Mange, M.: Depositional and structural
1111 evolution of a foreland basin margin in a magnetostratigraphic framework: the eastern Swiss
1112 Molasse Basin, International Journal of Earth Sciences, 88, 253-275, 1999.

1113 Kissling, E., and Schlunegger, F.: Rollback orogeny model for the evolution of the Swiss
1114 Alps, Tectonics, 37, 1097-1115, 2018.

1115 Krawczyk, C., McCann, T., Cocks, L.R.M., England, R.W., McBride, J.H. and
1116 Wybraniec, S.: Caledonian tectonics, In The Geology of Central Europe (McCann, T., Ed.), 1,
1117 Precambrian and Paleozoic, Geological Society, London, 303-381, 2008.

1118 Kröner, A., and Stern, R.: AFRICA| Pan-African orogeny, 2005.

1119 Krippner, A., and Bahlburg, H.: Provenance of Pleistocene Rhine River Middle Terrace
1120 sands between the Swiss–German border and Cologne based on U–Pb detrital zircon ages,
1121 International Journal of Earth Sciences, 102, 917-932, 2013.

1122 Kuhlemann, J.: Post-collisional sediment budget of circum-Alpine basins (Central
1123 Europe), Mem. Sci. Geol. Padova, 52, 1-91, 2000.

1124 Kuhlemann, J., and Kempf, O.: Post-Eocene evolution of the North Alpine Foreland
1125 Basin and its response to Alpine tectonics, Sedimentary Geology, 152, 45-78, 2002.

1126 Kühni, A., and Pfiffner, O.-A.: Drainage patterns and tectonic forcing: a model study for
1127 the Swiss Alps, Basin Research, 13, 169-197, 2001.

1128 Kylander-Clark, A. R. C., Hacker, B. R., and Cottle, J. M.: Laser-ablation split-stream
1129 ICP petrochronology, Chemical Geology, 345, 99-112, 10.1016/j.chemgeo.2013.02.019, 2013.

1130 Laubscher, H.: Detachment, shear, and compression in the central Alps, Geol. Soc. Am.
1131 Mem, 158, 191-211, 1983.

1132 Lihou, J. C., and Allen, P. A.: Importance of inherited rift margin structures in the early
1133 North Alpine Foreland Basin, Switzerland, Basin Research, 8, 425-442, 1996.

1134 Lippitsch, R., Kissling, E., and Ansorge, J.: Upper mantle structure beneath the Alpine
1135 orogen from high-resolution teleseismic tomography, Journal of Geophysical Research: Solid
1136 Earth, 108, 2003.

1137 Lu, G., Winkler, W., Rahn, M., von Quadt, A., and Willett, S. D.: Evaluating igneous
1138 sources of the Taveyannaz formation in the Central Alps by detrital zircon U–Pb age dating and
1139 geochemistry, *Swiss Journal of Geosciences*, 111, 399-416, 2018.

1140 Mair, D., Lechmann, A., Herwegh, M., Nibourel, L., and Schlunegger, F.: Linking Alpine
1141 deformation in the Aar Massif basement and its cover units—the case of the Jungfrau–Eiger
1142 mountains (Central Alps, Switzerland), *Solid Earth*, 9, 1099-1122, 2018.

1143 Malusa, M. G., Anfinson, O. A., Dafov, L. N., and Stockli, D. F.: Tracking Adria
1144 indentation beneath the Alps by detrital zircon U-Pb geochronology: Implications for the
1145 Oligocene-Miocene dynamics of the Adriatic microplate, *Geology*, 44, 155-158,
1146 10.1130/G37407.1, 2016.

1147 Mancktelow, N.: The Simplon Line: a major displacement zone in the western Lepontine
1148 Alps, *Eclogae Geol Helv*, 78, 73-96, 1985.

1149 Mancktelow, N. S., and Grasemann, B.: Time-dependent effects of heat advection and
1150 topography on cooling histories during erosion, *Tectonophysics*, 270, 167-195, 1997.

1151 Marsh, J. H., and Stockli, D. F.: Zircon U–Pb and trace element zoning characteristics in
1152 an anatexitic granulite domain: Insights from LASS-ICP-MS depth profiling, *Lithos*, 239, 170-
1153 185, 2015.

1154 Matter, A.: Sedimentologische Untersuchungen im östlichen Napfgebiet (Entlebuch—Tal
1155 der Grossen Fontanne, Kt. Luzern): *Eclogae Geologicae Helvetiae*, 57, 315–428, 1964.

1156 Matter, A., Homewood, P. W., Caron, C., Van Stuijvenberg, J., Weidmann, M., and
1157 Winkler, W.: Flysch and molasse of central and western Switzerland, in Trümpy, R., ed.,
1158 *Geology of Switzerland, a guide book: Schweiz Geologica Kommission*, 261–293, 1980.

1159 Mazurek, M., Hurford, A. J., and Leu, W.: Unravelling the multi-stage burial history of
1160 the Swiss Molasse Basin: integration of apatite fission track, vitrinite reflectance and biomarker
1161 isomerisation analysis, *Basin Research*, 18, 27-50, 2006.

1162 McCann, T. (Ed.): *The geology of central Europe*, Geol. Soc. London, 2008.

1163 Müller, B., Schaltegger, U., Klötzli, U., and Flisch, M.: Early Cambrian oceanic
1164 plagiogranite in the Silvretta nappe, eastern Alps: Geochemical, zircon U-Pb and Rb-Sr data
1165 from garnet-hornblende-plagioclase gneisses, *Geologische Rundschau*, 85, 822-831, 1996.

1166 Neubauer, F.: Evolution of late Neoproterozoic to early Paleozoic tectonic elements in
1167 Central and Southeast European Alpine mountain belts: review and synthesis, *Tectonophysics*,
1168 352, 87-103, 2002.

1169 Niggli, E., and Niggli, C.: Karten der Verbreitung einiger Mineralien der alpidischen
1170 Metamorphose in den Schweizer Alpen (Stilpnomelan, Alkali-Amphibol, Chloritoid, Staurolith,
1171 Disthen, Sillimanit), *Eclogae Geol Helv*, 58, 335-368, 1965.

1172 Oberhauser, R.: 110 St. Galen Nord Und 111 Dornbern Nord, Geologische
1173 Bundesanstalt, Vienna, AT, 1994.

1174 Paton, C., Hellstrom, J., Paul, B., Woodhead, J., and Hergt, J.: Iolite: Freeware for the
1175 visualisation and processing of mass spectrometric data, *Journal of Analytical Atomic*
1176 *Spectrometry*, 26, 2508-2518, 2011.

1177 Pazzaglia, F. J., Selverstone, J., Roy, M., Steffen, K., Newland-Pearce, S., Knipscher, W.,
1178 and Pearce, J.: Geomorphic expression of midcrustal extension in convergent orogens, *Tectonics*,
1179 26, 2007.

1180 Petrus, J. A., and Kamber, B. S.: VizualAge: A Novel Approach to Laser Ablation ICP-
1181 MS U-Pb Geochronology Data Reduction, *Geostandards and Geoanalytical Research*, 36, 247-
1182 270, 10.1111/j.1751-908X.2012.00158.x, 2012.

1183 Pfiffner, O.-A., Schlunegger, F., and Buiter, S.: The Swiss Alps and their peripheral
1184 foreland basin: Stratigraphic response to deep crustal processes, *Tectonics*, 21, 3-1-3-16, 2002.

1185 Pfiffner, O. A.: Evolution of the north Alpine foreland basin in the Central Alps, *Foreland*
1186 *basins*, 219-228, 1986.

1187 Pfiffner, O. A.: *Geology of the Alps*, John Wiley & Sons, 2014.

1188 Platt, N. H., and Keller, B.: Distal alluvial deposits in a foreland basin setting—the Lower
1189 *Freshwater Miocene*, Switzerland: sedimentology, architecture and palaeosols, *Sedimentology*,
1190 39, 545-565, 1992.

1191 Rahn, M., Mullis, J., Erdelbrock, K., and Frey, M.: Very low-grade metamorphism of the
1192 Taveyanne greywacke, Glarus Alps, Switzerland, *Journal of Metamorphic Geology*, 12, 625-641,
1193 1994.

1194 Reichenwallner, S.: Die vulkanische Aktivität in den Westalpen hergeleitet aus
1195 detritischem Amphibol und Klinopyroxen im Taveyannaz-Sandstein, unpublished Ms thesis,
1196 University of Bern, Bern, 57 pp., 2019.

1197 Renz, H.: Die subalpine Molasse zwischen Aare und Rhein, 1937.

1198 Ring, U.: The Alpine geodynamic evolution of Penninic nappes in the eastern Central
1199 Alps: geothermobarometric and kinematic data, *Journal of Metamorphic Geology*, 10, 33-53,
1200 1992.

1201 Rubatto, D.: Zircon trace element geochemistry: partitioning with garnet and the link
1202 between U–Pb ages and metamorphism, *Chemical geology*, 184, 123-138, 2002.

1203 Rubatto, D., Regis, D., Hermann, J., Boston, K., Engi, M., Beltrando, M., and McAlpine,
1204 S. R.: Yo-yo subduction recorded by accessory minerals in the Italian Western Alps, *Nature*
1205 *Geoscience*, 4, 338-342, 2011.

1206 Schaad W., Keller, B., and Matter A.: Die Obere Meeresmolasse (OMM) am Pfänder:
1207 Beispiel eines Gilbert-Deltakomplexes, *Eclogae Geol. Helv.*, 85, 145–168, 1992.

1208 Schaltegger, U.: Unravelling the pre-Mesozoic history of Aar and Gotthard massifs
1209 (Central Alps) by isotopic dating: a review: The pre-Alpine crustal evolution of the Aar-,
1210 Gotthard-and Tavetsch massifs, *Schweizerische Mineralogische und Petrographische*
1211 *Mitteilungen*, 74, 41-51, 1994.

1212 Schaltegger, U., and Gebauer, D.: Pre-Alpine geochronology of the central, western and
1213 southern Alps, *Schweizerische Mineralogische und Petrographische Mitteilungen*, 79, 79-87,
1214 1999.

1215 Schaltegger, U., Abrecht, J., and Corfu, F.: The Ordovician orogeny in the Alpine
1216 basement: constraints from geochronology and geochemistry in the Aar Massif (Central Alps),
1217 *Swiss Bulletin of Mineralogy and Petrology*, 83, 183-239, 2003.

1218 Schegg, R., Cornford, C., and Leu, W.: Migration and accumulation of hydrocarbons in
1219 the Swiss Molasse Basin: implications of a 2D basin modeling study, *Mar Petrol Geol*, 16, 511-
1220 531, 1999.

1221 Schlanke, S.: *Geologie Der Subalpinen Molasse Zwischen Biberbrugg SZ, Huetten ZH*
1222 *Und Agerisee ZG, Schweiz*, 1974.

1223 Schlunegger, F., Matter, A., and Mange, M. A.: Alluvial fan sedimentation and structure
1224 of the southern Molasse basin margin, Lake Thun area, Switzerland, *Eclogae Geol. Helv.*, 86,
1225 717–750, 1993.

1226 Schlunegger, F., Burbank, D. W., and Matter, A.: Magnetostratigraphic calibration of the
1227 Oligocene to Middle Miocene (30-15 Ma) mammal biozones and depositional sequences of the
1228 Swiss Molasse Basin, *Eclogae Geol Helv*, 89, 753-788, 1996.

1229 Schlunegger, F., Matter, A., Burbank, D. W., and Klaper, E. M.: Magnetostratigraphic
1230 constraints on relationships between evolution of the central Swiss Molasse basin and Alpine
1231 orogenic events, *Geological Society of America Bulletin*, 102, 225-241, 1997a.

1232 Schlunegger, F., Leu, W., and Matter, A.: Sedimentary sequences, seismic facies,
1233 subsidence analysis, and evolution of the Burdigalian Upper Marine Molasse Group, central
1234 Switzerland, *AAPG bulletin*, 81, 1185-1207, 1997b.

1235 Schlunegger, F., Matter, A., Burbank, D., Leu, W., Mange, M., and Matyas, J.:
1236 Sedimentary sequences, seismofacies and evolution of depositional systems of the
1237 Oligo/Miocene Lower Freshwater Molasse Group, Switzerland, *Basin Research*, 9, 1-26, 1997c.

1238 Schlunegger, F., Slingerl, R., and Matter, A.: Crustal thickening and crustal extension as
1239 controls on the evolution of the drainage network of the central Swiss Alps between 30 Ma and
1240 the present: constraints from the stratigraphy of the North Alpine Foreland Basin and the
1241 structural evolution of the Alps, *Basin Research*, 10, 197-212, 1998.

1242 Schlunegger, F., and Willett, S.: Spatial and temporal variations in exhumation of the
1243 central Swiss Alps and implications for exhumation mechanisms, *Geological Society, London,*
1244 *Special Publications*, 154, 157-179, 1999.

1245 Schlunegger, F., Rieke-Zapp, D., and Ramseyer, K.: Possible environmental effects on
1246 the evolution of the Alps-Molasse Basin system, *Swiss Journal of Geosciences*, 100, 383-405,
1247 10.1007/s00015-007-1238-9, 2007.

1248 Schlunegger, F., and Norton, K. P.: Water versus ice: The competing roles of modern
1249 climate and Pleistocene glacial erosion in the Central Alps of Switzerland, *Tectonophysics*, 602,
1250 370-381, 2013.

1251 Schlunegger, F., and Kissling, E.: Slab rollback orogeny in the Alps and evolution of the
1252 Swiss Molasse basin, *Nature communications*, 6, 1-10, 2015.

1253 Schlunegger, F., and Castelltort, S.: Immediate and delayed signal of slab breakoff in
1254 Oligo/Miocene Molasse deposits from the European Alps, *Scientific reports*, 6, 31010, 2016.

1255 Schmid, S., Aebli, H., Heller, F., and Zingg, A.: The role of the Periadriatic Line in the
1256 tectonic evolution of the Alps, Geological Society, London, Special Publications, 45, 153-171,
1257 1989.

1258 Schmid, S. M., Pfiffner, O. A., Froitzheim, N., Schönborn, G., and Kissling, E.:
1259 Geophysical-geological transect and tectonic evolution of the Swiss-Italian Alps, Tectonics, 15,
1260 1036-1064, 10.1029/96tc00433, 1996.

1261 Schmid, S. M., Fugenschuh, B., Kissling, E., and Schuster, R.: Tectonic map and overall
1262 architecture of the Alpine orogen, Eclogae Geol Helv, 97, 93-117, 10.1007/s00015-004-1113-x,
1263 2004.

1264 Sharman, G. R., Hubbard, S. M., Covault, J. A., Hinsch, R., Linzer, H. G., and Graham,
1265 S. A.: Sediment routing evolution in the North Alpine Foreland Basin, Austria: interplay of
1266 transverse and longitudinal sediment dispersal, Basin Research, 30, 426-447, 2018a.

1267 Sharman, G. R., Sharman, J. P., and Sylvester, Z.: detritalPy: A Python-based toolset for
1268 visualizing and analysing detrital geo-thermochronologic data, The Depositional Record, 4, 202-
1269 215, 2018b.

1270 Sinclair, H., and Allen, P.: Vertical versus horizontal motions in the Alpine orogenic
1271 wedge: stratigraphic response in the foreland basin, Basin Research, 4, 215-232, 1992.

1272 Sinclair, M. R., Wratt, D. S., Henderson, R. D., and Gray, W. R.: Factors affecting the
1273 distribution and spillover of precipitation in the Southern Alps of New Zealand—A case study,
1274 Journal of Applied Meteorology, 36, 428-442, 1997.

1275 Soto-Kerans, G. M., Stockli, D. F., Janson, X., Lawton, T. F., and Covault, J. A.: Orogen
1276 proximal sedimentation in the Permian foreland basin, Geosphere, 2020.

1277 Spicher, A.: Tektonische Karte der Schweiz: 1: 500 000, Schweizerische Geologische
1278 Kommission Bern, 1980.

1279 Spiegel, C., Kuhlemann, J., Dunkl, I., Frisch, W., Von Eynatten, H., and Balogh, K.: The
1280 erosion history of the Central Alps: evidence from zircon fission track data of the foreland basin
1281 sediments, Terra Nova, 12, 163-170, 2000.

1282 Spiegel, C., Kuhlemann, J., Dunkl, I., and Frisch, W.: Paleogeography and catchment
1283 evolution in a mobile orogenic belt: the Central Alps in Oligo–Miocene times, Tectonophysics,
1284 341, 33-47, 2001.

1285 Spiegel, C., Siebel, W., Frisch, W., and Berner, Z.: Nd and Sr isotopic ratios and trace
1286 element geochemistry of epidote from the Swiss Molasse Basin as provenance indicators:
1287 implications for the reconstruction of the exhumation history of the Central Alps, *Chemical*
1288 *Geology*, 189, 231-250, 2002.

1289 Spiegel, C., Siebel, W., Kuhlemann, J., and Frisch, W.: Toward a comprehensive
1290 provenance analysis: A multi-method approach and its implications for the evolution of the
1291 Central Alps, *Special Papers-Geological Society of America*, 37-50, 2004.

1292 Stampfli, G. M., and Borel, G. D.: A plate tectonic model for the Paleozoic and Mesozoic
1293 constrained by dynamic plate boundaries and restored synthetic oceanic isochrons, *Earth and*
1294 *Planetary Science Letters*, 196, 17-33, Doi 10.1016/S0012-821x(01)00588-X, 2002.

1295 Steck, A., Della Torre, F., Keller, F., Pfeifer, H.-R., Hunziker, J., and Masson, H.:
1296 Tectonics of the Lepontine Alps: ductile thrusting and folding in the deepest tectonic levels of
1297 the Central Alps, *Swiss Journal of Geosciences*, 106, 427-450, 2013.

1298 Steiger, R. H., and Jäger, E.: Subcommittee on geochronology: convention on the use of
1299 decay constants in geo- and cosmo-chronology, *Earth and planetary science letters*, 36, 359-362,
1300 1977.

1301 Stephan, T., Kroner, U., Romer, R. L., and Rösel, D.: From a bipartite Gondwana shelf to
1302 an arcuate Variscan belt: The early Paleozoic evolution of northern Peri-Gondwana, *Earth-*
1303 *science reviews*, 2019.

1304 Stephan, T., Kroner, U., and Romer, R. L.: The pre-orogenic detrital zircon record of the
1305 Peri-Gondwanan crust, *Geological Magazine*, 156, 281-307, 2019b.

1306 Strunck, P., and Matter, A.: Depositional evolution of the western Swiss Molasse,
1307 *Eclogae Geol Helv*, 95, 197-222, 2002.

1308 Stürm, B.: Die Rigischüttung. Sedimentpetrographie, Sedimentologie, Paläogeographie,
1309 Tektonik [Ph.D. dissert.], Zürich, Switzerland, Universität Zürich, 98 p., 1973.

1310 Stutenbecker, L., Tollan, P. M., Madella, A., and Lanari, P.: Miocene basement
1311 exhumation in the Central Alps recorded by detrital garnet geochemistry in foreland basin
1312 deposits, *Solid Earth*, 10, 1581-1595, 2019.

1313 Trümpy, R., Aubert, D., and Bernoulli, D.: *Geology of Switzerland: Geological*
1314 *excursions*, Wepf, 1980.

1315 Vermeesch, P.: How many grains are needed for a provenance study?, *Earth and*
1316 *Planetary Science Letters*, 224, 441-451, 10.1016/j.epsl.2004.05.037, 2004.

1317 Vermeesch, P.: Dissimilarity measures in detrital geochronology, *Earth-Science Reviews*,
1318 178, 310-321, 2018.

1319 Vernon, A. J., van der Beek, P. A., and Sinclair, H. D.: Spatial correlation between long-
1320 term exhumation rates and present-day forcing parameters in the western European Alps,
1321 *Geology*, 37, 859-862, 2009.

1322 Von Eynatten, H., Schlunegger, F., Gaupp, R., and Wijbrans, J. R.: Exhumation of the
1323 Central Alps: evidence from $^{40}\text{Ar}/^{39}\text{Ar}$ laserprobe dating of detrital white micas from the Swiss
1324 Molasse Basin, *Terra Nova*, 11, 284-289, 1999.

1325 Von Eynatten, H., and Wijbrans, J.: Precise tracing of exhumation and provenance using
1326 $^{40}\text{Ar}/^{39}\text{Ar}$ geochronology of detrital white mica: the example of the Central Alps, *Geological*
1327 *Society, London, Special Publications*, 208, 289-305, 2003.

1328 von Eynatten, H., and Dunkl, I.: Assessing the sediment factory: the role of single grain
1329 analysis, *Earth-Science Reviews*, 115, 97-120, 2012.

1330 von Raumer, J.: The Palaeozoic evolution in the Alps: from Gondwana to Pangea,
1331 *Geologische Rundschau*, 87, 407-435, 1998.

1332 von Raumer, J. F., Stampfli, G. M., Borel, G., and Bussy, F.: Organization of pre-
1333 Variscan basement areas at the north-Gondwanan margin, *International Journal of Earth*
1334 *Sciences*, 91, 35-52, 10.1007/s005310100200, 2002.

1335 von Raumer, J. F., Stampfli, G. M., and Bussy, F.: Gondwana-derived microcontinents—
1336 the constituents of the Variscan and Alpine collisional orogens, *Tectonophysics*, 365, 7-22, 2003.

1337 von Raumer, J. F., Bussy, F., and Stampfli, G. M.: The Variscan evolution in the External
1338 massifs of the Alps and place in their Variscan framework, *Comptes Rendus Geoscience*, 341,
1339 239-252, 2009.

1340 Wiederkehr, M., Sudo, M., Bousquet, R., Berger, A., and Schmid, S. M.: Alpine orogenic
1341 evolution from subduction to collisional thermal overprint: The $^{40}\text{Ar}/^{39}\text{Ar}$ age constraints from
1342 the Valaisan Ocean, central Alps, *Tectonics*, 28, 2009.

1343 Willett, S. D., and Schlunegger, F.: The last phase of deposition in the Swiss Molasse
1344 Basin: From foredeep to negative-alpha basin, *Basin Research*, 22, 623-639, 2010.

1345 Zurbriggen, R.: The Cenerian orogeny (early Paleozoic) from the perspective of the
1346 Alpine region, *International Journal of Earth Sciences*, 106, 517-529, 2017.

1347 Zweigel, J., Aigner, T., and Luterbacher, H.: Eustatic versus tectonic controls on Alpine
1348 foreland basin fill: sequence stratigraphy and subsidence analysis in the SE German Molasse,
1349 Geological Society, London, Special Publications, 134, 299-323, 1998.

Table 1

Sample Name	Unit of SMB	Latitude	Longitude	Elevation (M)	Dep. Age (Ma)	+/- (Ma)	U-Pb	Geochem	Loc. of Analysis
Thun, CH									
OA13-SFB03	LFM I	46.789815	7.711673	740	27	0.5	x		UT
OA13-SFB04	LFM I	46.783249	7.730281	840	26	0.5	x		UT
10SMB06	LFM II	46.77989	7.6556	689	23	2.5	x		KU
10SMB07	UFM	46.81503	7.65013	689	18	3	x		KU
Lucerne, CH									
09-SFB-38	UFM	47.14054	8.19664	461	13.5	1	x	x	UT
09-SFB-11	UFM	47.10245	8.35003	420	14	1	x		KU
09-SFB-07	UFM	47.0569	8.24923	478	15.5	1	x		UT
09-SFB-12	UFM	47.10245	8.35003	420	16	1	x		UT
09-SFB-14	UMM	47.06692	8.32032	476	17.5	1	x	x	UT
09-SFB-49	UMM	47.02051	8.2403	676	19	1	x	x	UT
09-SFB-29	UMM	47.06442	8.32369	498	19	1	x		KU
09-SFB-05	UMM	47.05639	8.31036	398	20	1	x		UT
09-SFB-33	LFM IIb	47.05681	8.34139	503	21	1	x	x	UT and KU
09-SFB-08	LFM IIb	47.04211	8.32706	442	21.5	1	x		UT
09-SFB-13	LFM IIb	47.0565	8.38408	547	21.5	1	x		KU
09-SFB-21	LFM IIa	47.03422	8.35363	436	22.5	1	x	x	UT
09-SFB-45	LFM I	47.041	8.4614	1332	27	1	x	x	UT
09-SFB-10b	LMM	47.00933	8.29391	615	32	1	x		KU
09-SFB-43	NHF	46.87763	8.66345	496	35	3	x	x	
09-SFB-02	NHF	46.89991	8.6262	461	35	3	x		KU
Bregenz, AT									
10SMB09	UFM	47.53763	9.76789	609	15	2	x		UT
10SMB10	UMM	47.50168	9.79451	622	19	2	x		UT and KU
10SMB11	LFM II	47.48016	9.76906	442	22	2	x		UT
10SMB12	LMM	47.44407	9.78484	442	31	1	x		UT

Table 1. Sample Information. Depositional age errors are based on: Lucerne Section- Schlunegger et al. (1997a); Thun Section- Schlunegger et al. (1993; 1996); Bregenz Section- Oberhauser (1994), Kempf et al. (1999), and Schaad et al. (1992). 'X' in 'U-Pb' and 'Geochem' columns indicate data available for that sample. Final column indicates if samples were analyzed at either the University of Kansas (KU) or the University of Texas at Austin (UT). Errors for depositional ages are discussed in Section 3. Corresponding methods are found in the Section 4.

Figure 1

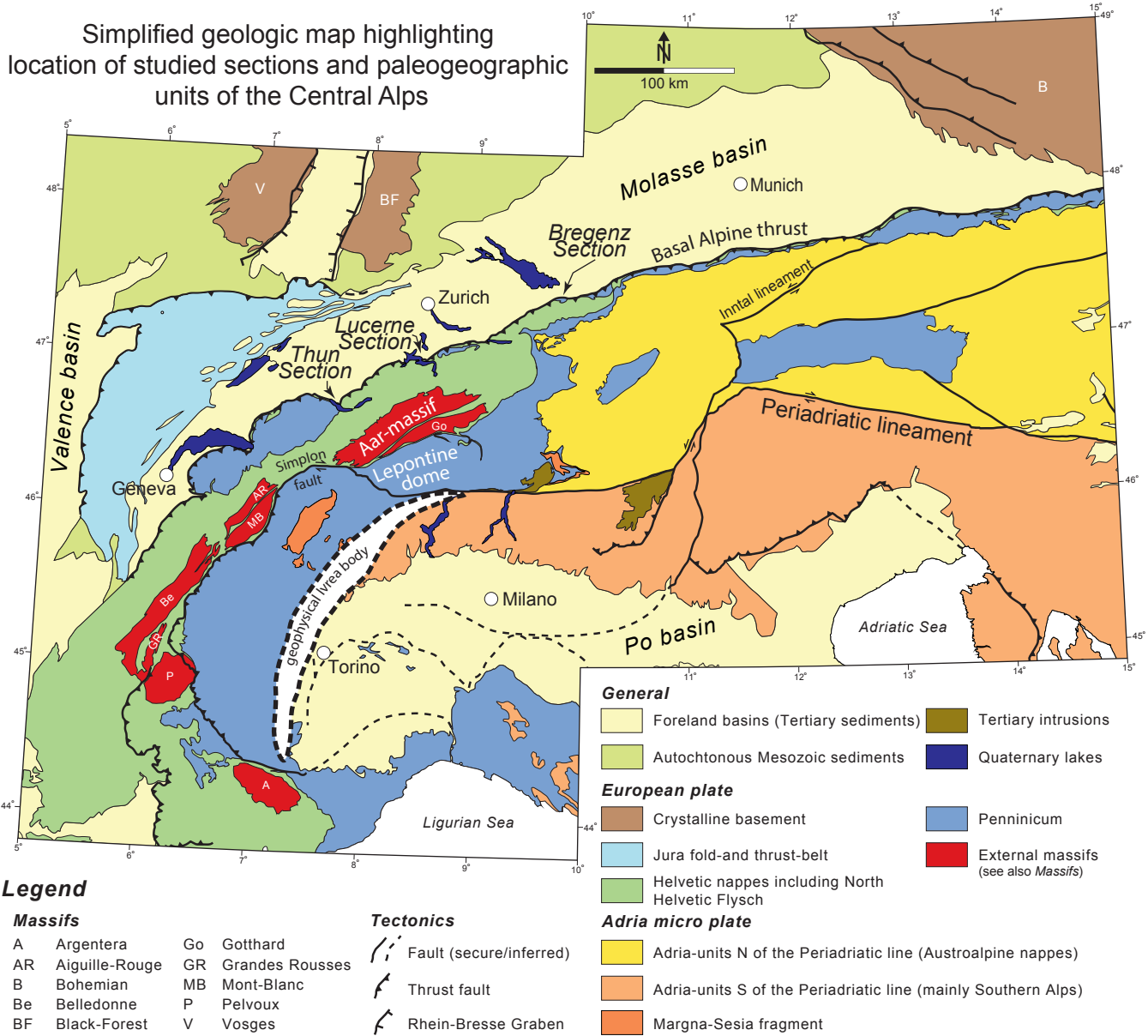


Figure 1. Geologic map of the Central Alps and Swiss Molasse Basin highlighting geologic features and paleogeographic units discussed in the text (map is adapted from Garefalakis and Schlunegger (2019) and based on: Froitzheim et al. (1996), Schmid et al. (2004), Handy et al. (2010), and Kissling and Schlunegger (2018)). Locations are shown for the Lucerne Section, Thun Section, and Bregenz Section that are highlighted in Figures 3a, 3b, and 3c, respectively.

Figure 2

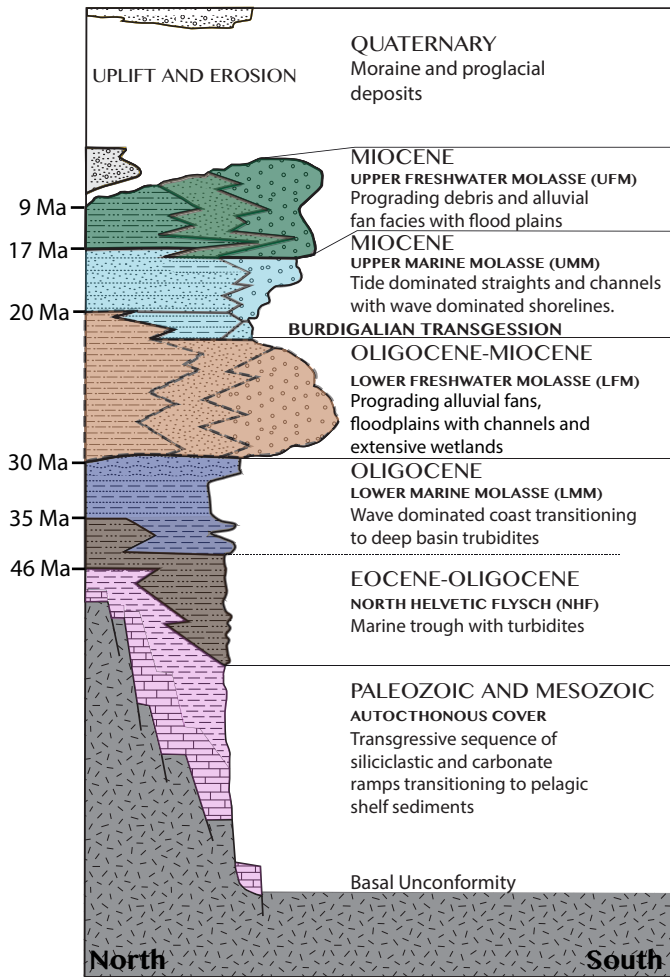


Figure 2. Generalized stratigraphy of the Molasse Basin. Modified from Miller (2009) and (Keller, 2000).

Figure 3

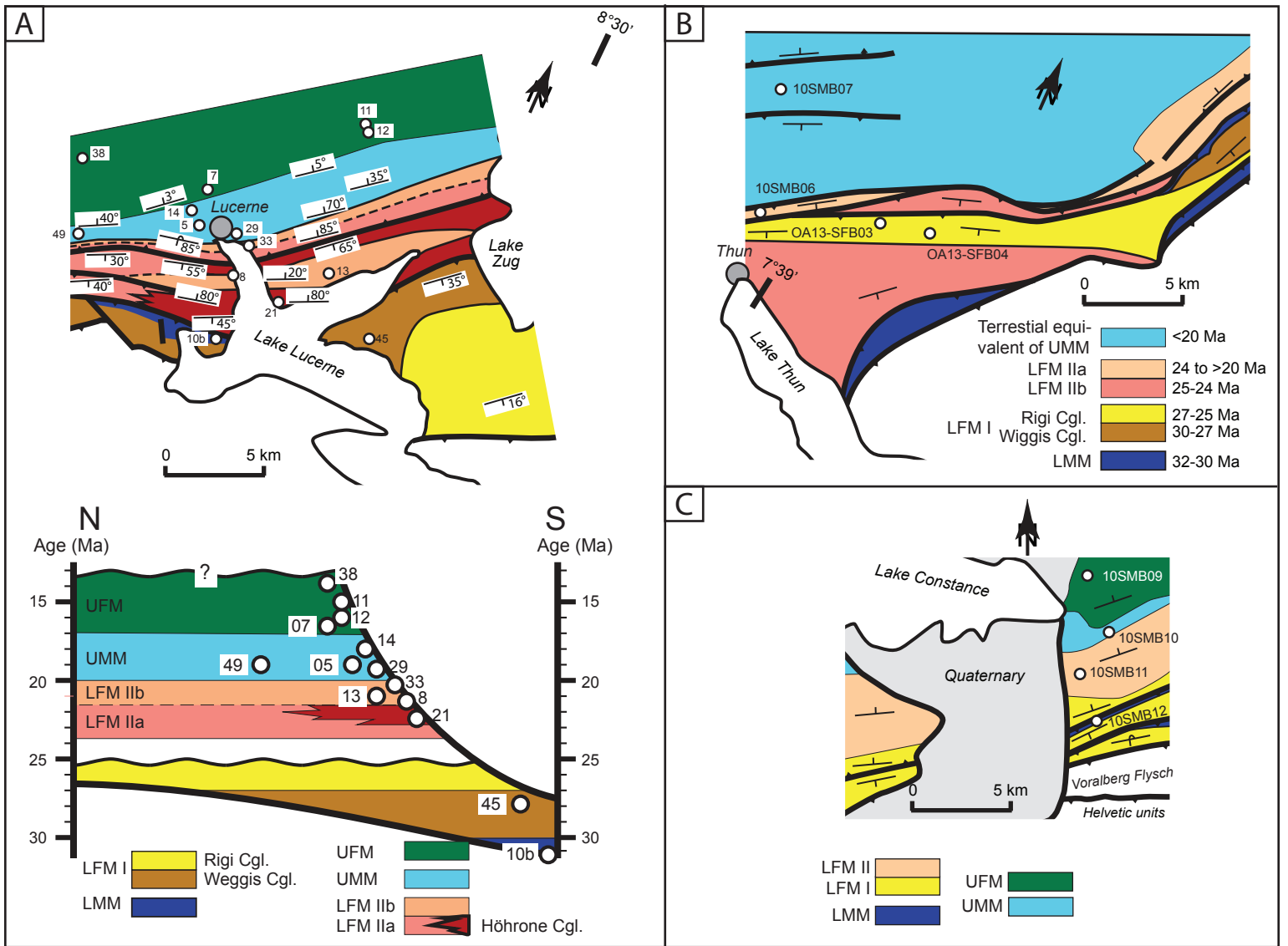


Figure 3. Stratigraphic units and sample locations of the three sampled sections A) Lucerne Section: geologic map and cross section modified from (Schlunegger et al., 1997a). In both the map and the simplified cross section, sample numbers are only the last two digits of the sample numbers from Table 1. B) Thun Section: geologic map modified from Schlunegger et al. (1993; 1996). C) Bregenz Section: geologic map simplified from Oberhauser, (1994), Kempf et al., (1999), and Schaad et al. (1992).

Figure 4

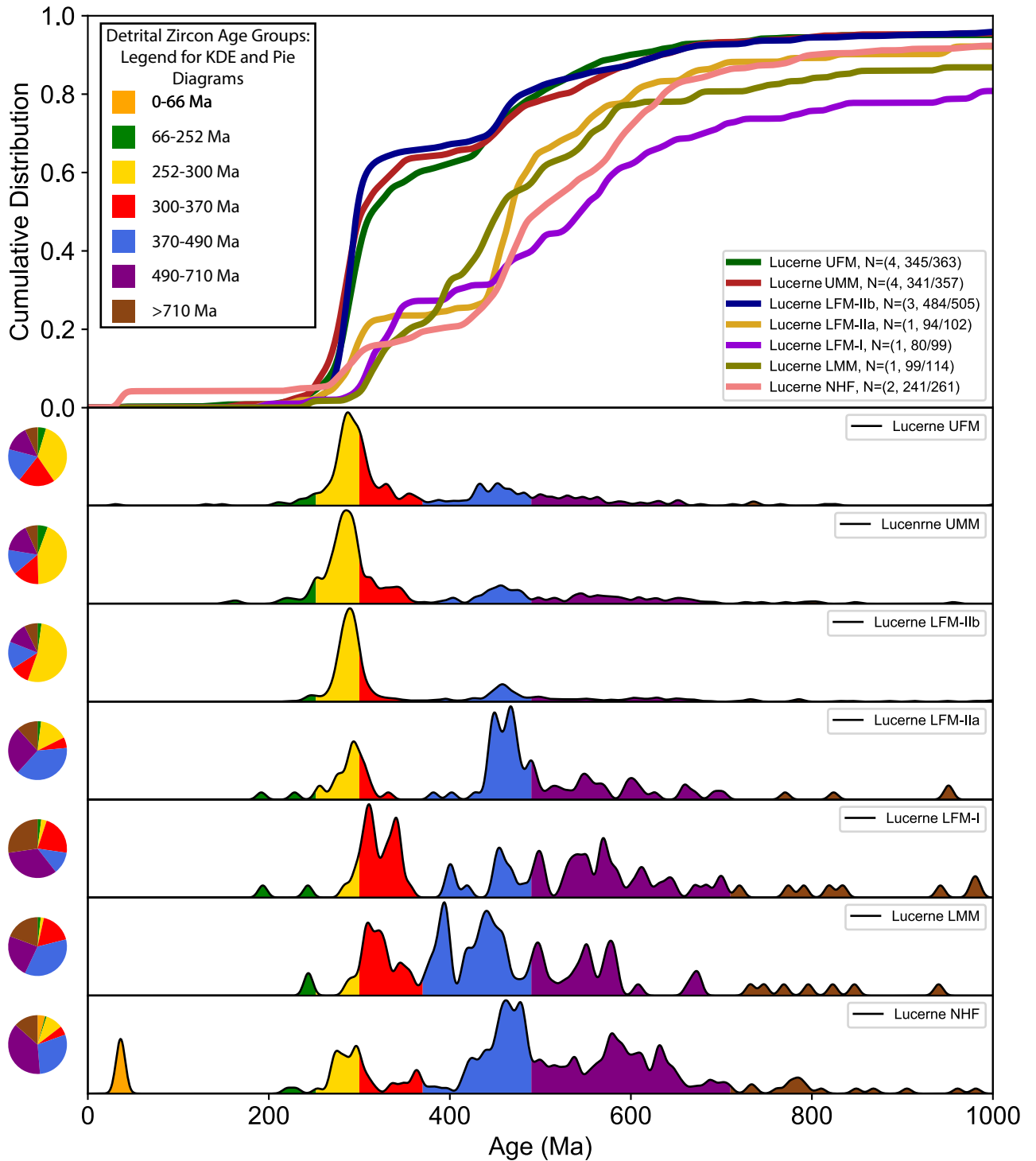


Figure 4. Detrital zircon U-Pb age data from the Lucerne Section (locations of samples depicted in Figure 3a) plotted as Kernel Density Estimations (KDE; Bandwidth set to 10), a Cumulative Distribution Plot (CDP), and as pie diagrams. Colored bars in the KDE and colored wedges in the pie diagrams show the relative abundance of age groups discussed in Section 5. Samples associated with each unit are referenced in Table 1. Plot only shows ages from 0-1000 Ma; however, a small number of older ages were analyzed and that data can be found in Supplemental File 1. N= (Number of samples, number of ages depicted/ total number of total ages).

Figure 5

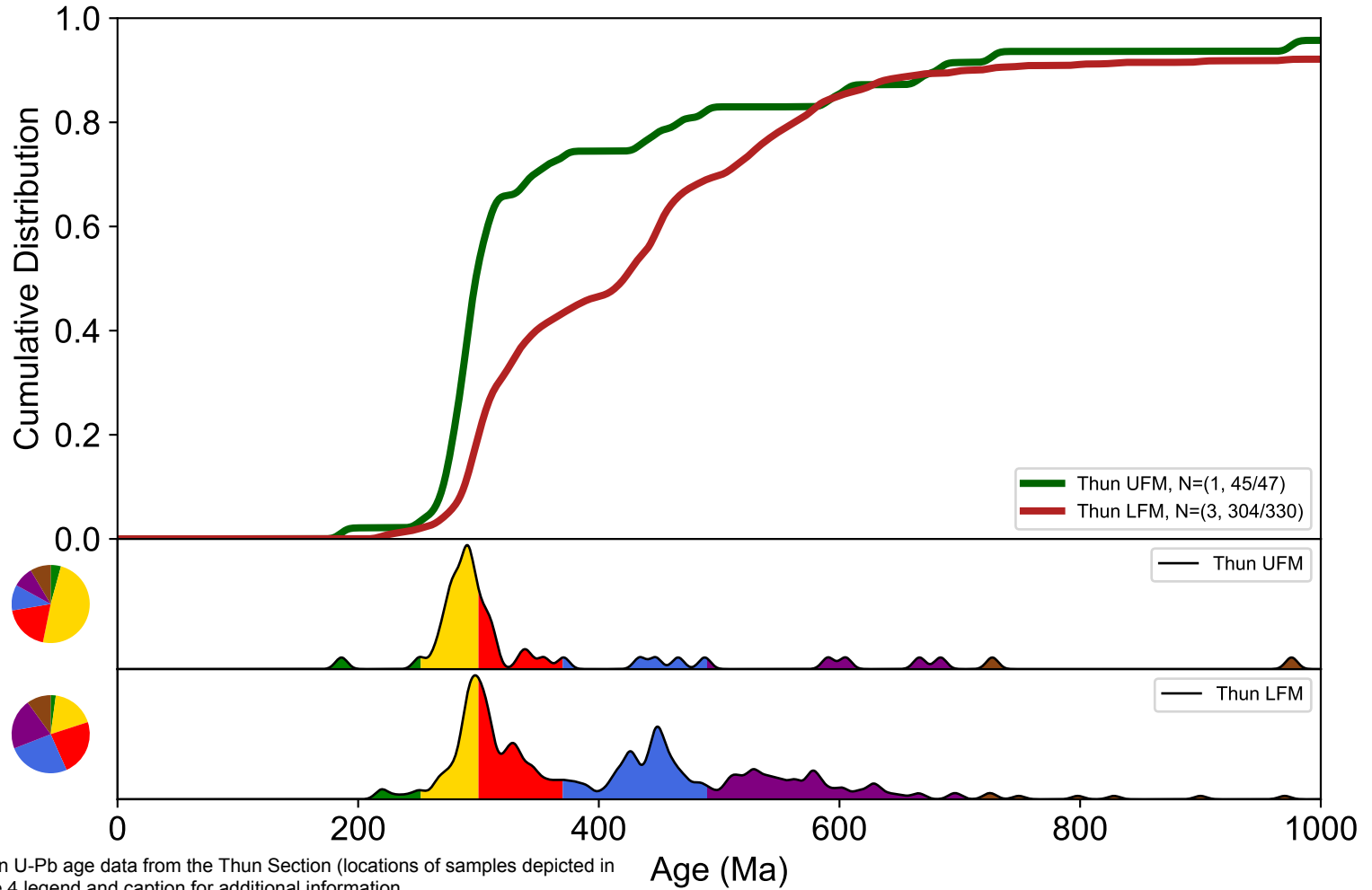


Figure 5. Detrital zircon U-Pb age data from the Thun Section (locations of samples depicted in Figure 3b). See Figure 4 legend and caption for additional information.

Figure 6

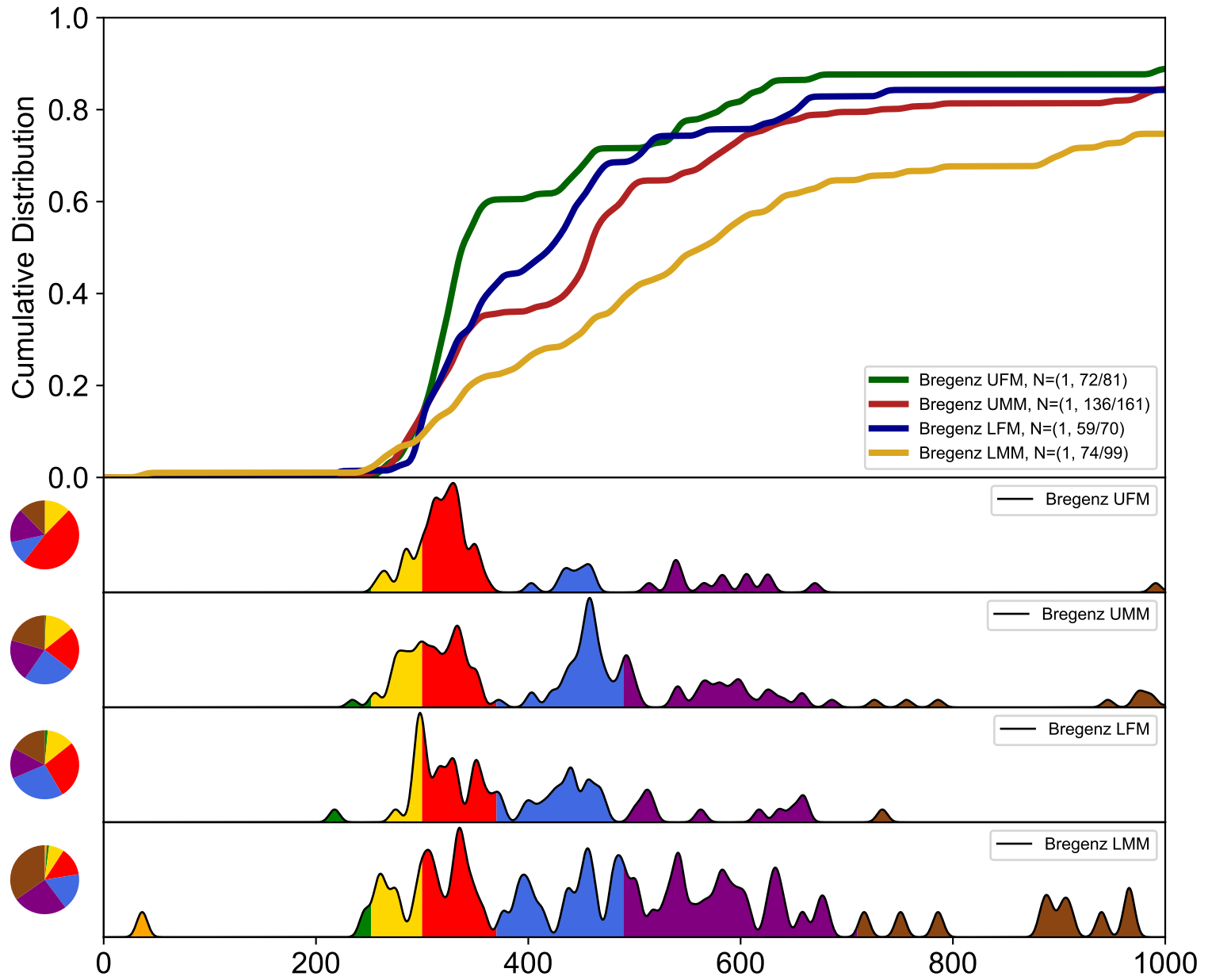


Figure 6. Detrital zircon U-Pb age data from the Bregenz Section (locations of samples depicted in Figure 3c). See Figure 4 legend and caption for additional information.

Age (Ma)

Figure 7

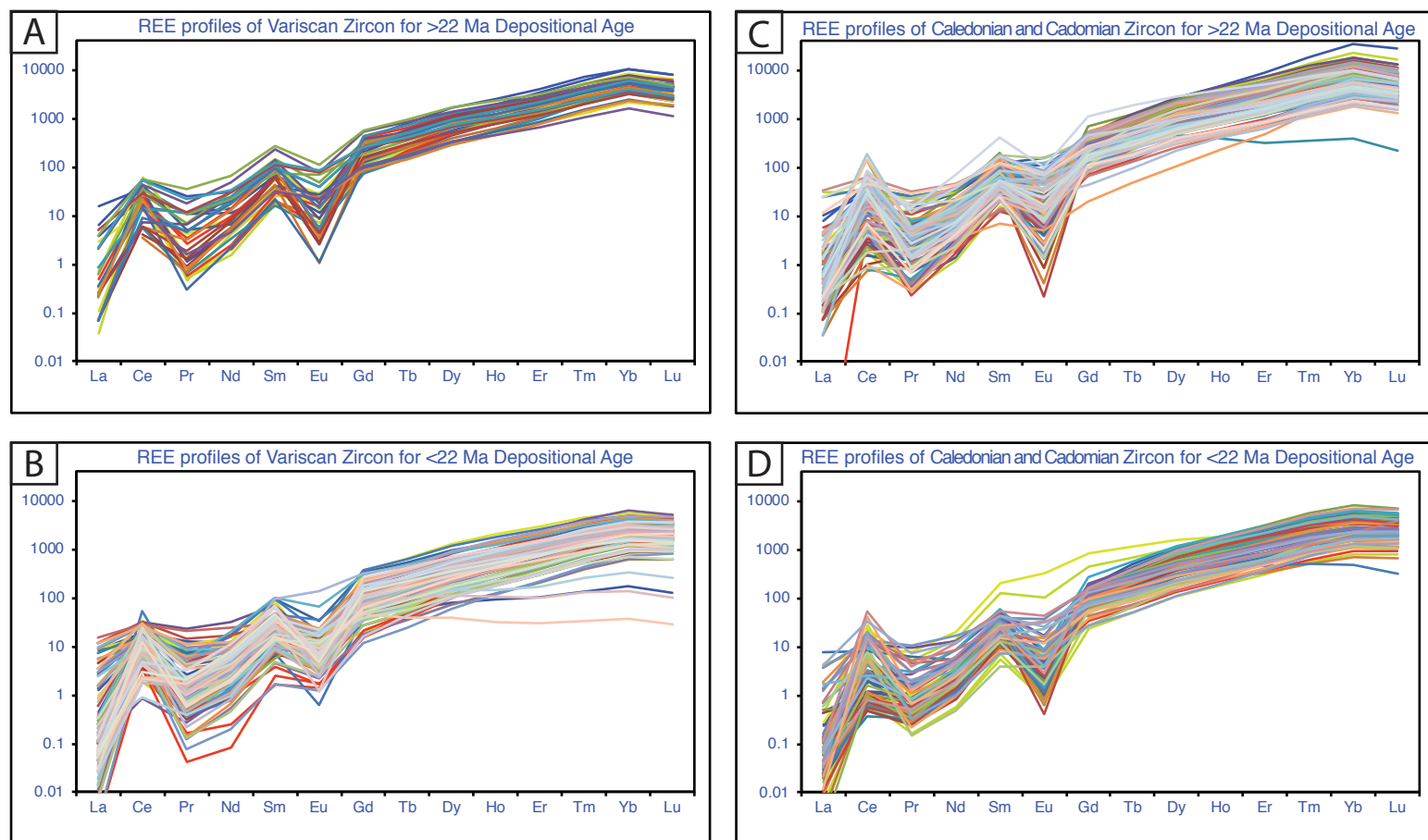


Figure 7. Detrital zircon Rare Earth Element (REE) spider diagram for samples collected from the Lucerne Section. (A) Variscan U-Pb ages and REE data for samples younger than a 22 Ma depositional age and (B) older than a 22 Ma depositional age. (C) Caledonian and Cadomian U-Pb ages and REE data for samples younger than a 22 Ma depositional age and (D) older than a 22 Ma depositional age. For plots A and C the geochemical data is drawn from samples SFB33 (21 Ma), SFB49 (19Ma), SFB14 (17.5 Ma), and SFB38 (13.5 Ma). For B and D the geochemical data is drawn from samples SFB21 (22.5 Ma) and SFB45 (27 Ma). The data suggest that detrital zircons from all three recent orogenic cycles record primarily grains that are magmatic in origin (Belousova et al., 2002; Hoskin and Ireland, 2000), with little evidence of metamorphic/metasomatic grains. Data can be found in Supplemental File 2.

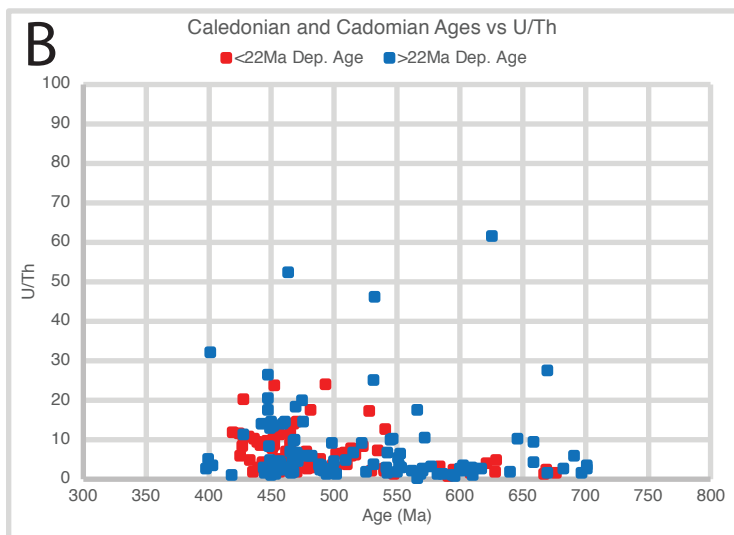
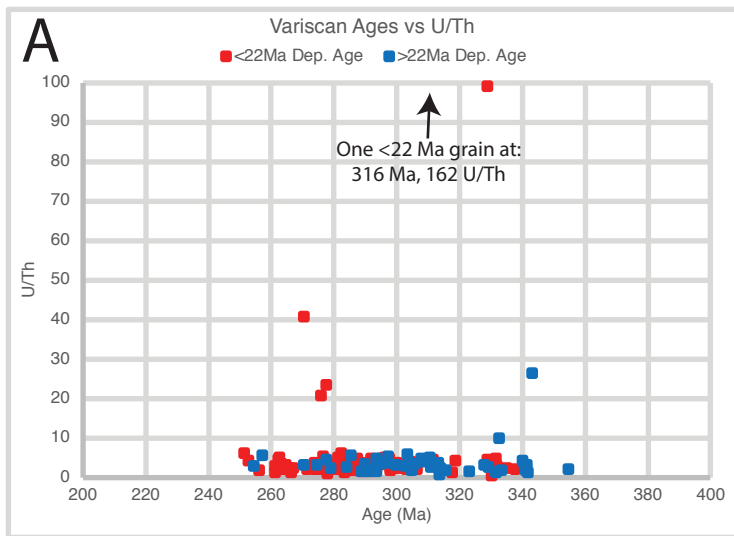


Figure 8

Figure 8. Age vs U/Th comparison for detrital zircon grains with depositional ages older than 22 Ma and younger than 22 Ma. A) Variscan aged grains, B) Caledonian and Cadomian age grains. Although not definitive, grains with elevated U/Th (or low Th/U; e.g. Rubatto et al. 2002) have a higher likelihood of being metamorphic in origin. There are few Variscan grains with elevated U/Th from both the pre- and post-22 Ma depositional ages, suggesting little input of metamorphic sources for these ages. There are a large number of Caledonian and a handful of Cadomian grains with elevated U/Th from both the pre- and post-22 Ma depositional ages, indicating metamorphic sources for these age grains are prevalent.

Figure 9

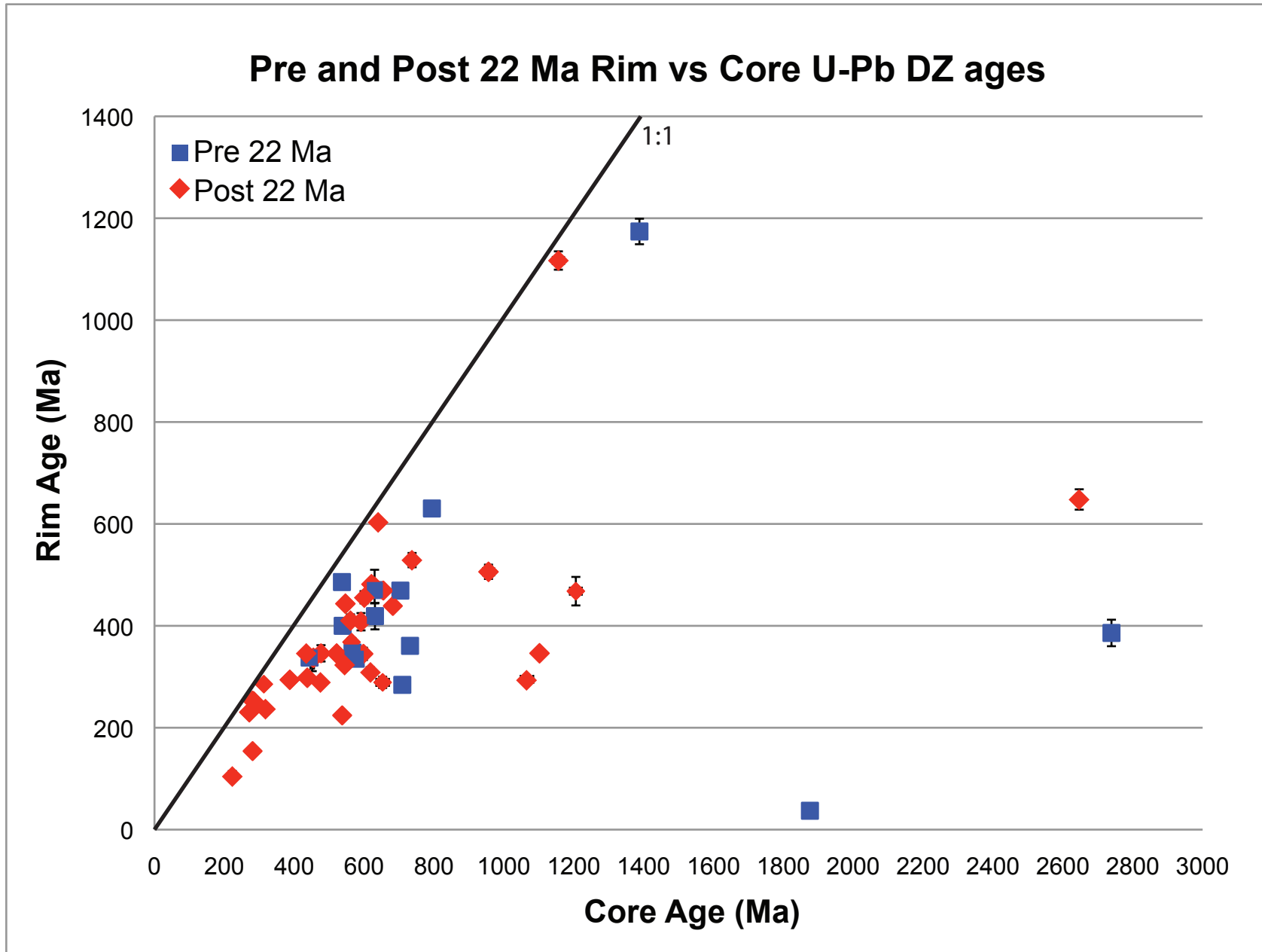


Figure 9. Rim vs core ages for detrital zircon grains from samples with depositional ages older than 22 Ma and younger than 22 Ma from the Lucerne Section. Prior to the 22 Ma transition in source area there is a minor number of Variscan rims on Cadomian and Caledonian cores. In samples younger than 22 Ma there is a noticeable increase in Variscan rims on Caledonian, Cadomian, and Proterozoic cores. Error bars are 2 sigma non-propagated errors.

Figure 10

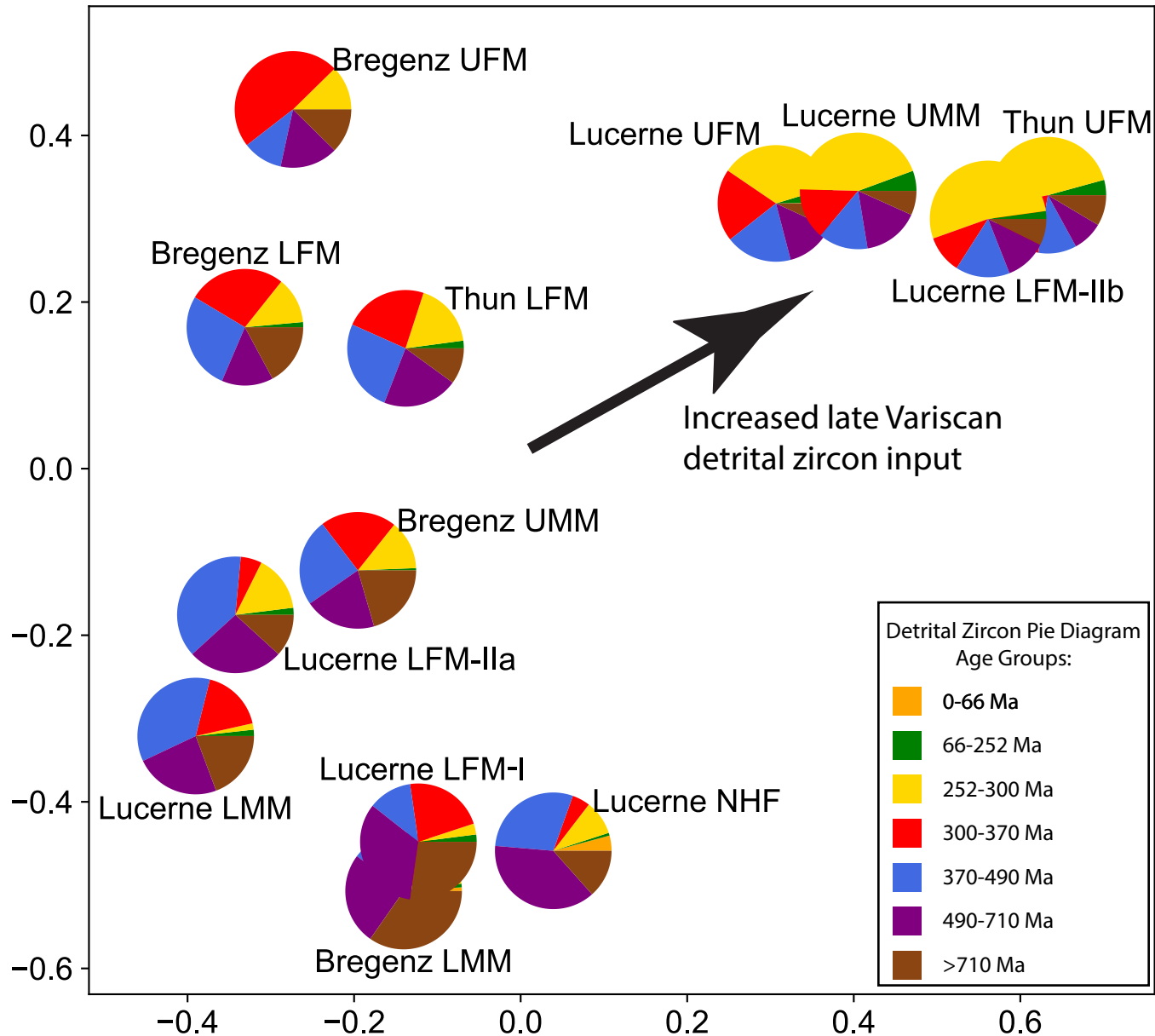


Figure 10. Multidimensional Scaling Plot (MDS) of detrital zircon U-Pb ages for all units from the Molasse Basin. The MDS plot was produced with the DetritalPy software of Sharman et al. (2018b) and is based on methods outlined by Vermeesch (2018). Pie diagram colors correspond to age groups from Figure 4 and ages discussed in Section 4.

Figure 11

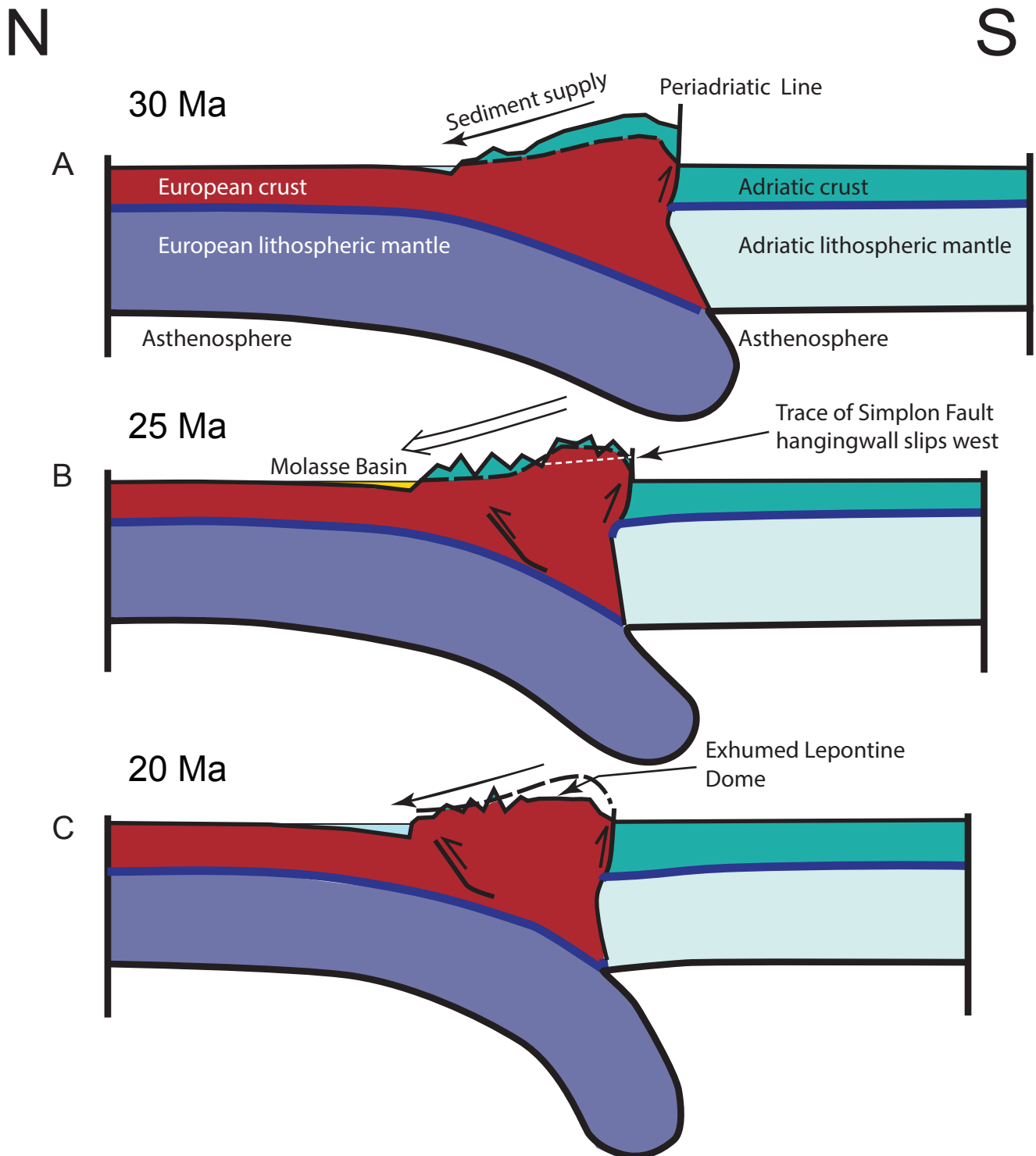


Figure 11. Schematic cross-section through the central Alps of Switzerland, illustrating the development of the Alpine relief and the topography through time. A) 30 Ma-25 Ma: Slab breakoff resulted in backthrusting along the Periadriatic fault and in the growth of the Alpine topography. The erosional hinterland was mainly made up of the Austroalpine cover nappes (Adriatic plate) and Penninic sedimentary rocks at the orogen front. B) 25 Ma: Ongoing surface erosion resulted in the formation of an Alpine-type landscape with valleys and mountains. First dissection into the crystalline core of the European continental plate was registered by the first arrival of Penninic crystalline material in the foreland basin sometime between 25 and 22 Ma, depending on the location within the basin. 22 Ma was also the time when sediment discharge to the Molasse was highest. Tectonic exhumation through slip along the Simplon fault started to occur at the highest rates. C) 20 Ma: Tectonic exhumation along the Simplon fault resulted in widespread exposure of high-grade rocks, in a shift in the clast suites of the conglomerates and in a change in the detrital zircon age signatures. Faulting along the detachment fault most likely subdued the topography in the hinterland. As a result, sediment flux to the Molasse basin decreased, and the basin became underfilled and was occupied by the peripheral sea of the Upper Marine Molasse. (Figures based on restored sections by Schlunegger and Kissling, 2015).